NATIONAL ADVISORY COMMITTEE FOR AERONAUTICS

TECHNICAL NOTE

No. 1134

DEVELOPMENT OF A PROTECTED AIR SCOOP FOR THE REDUCTION OF INDUCTION-SYSTEM ICING

By Uwe von Glahn and Clark E. Renner

Aircraft Engine Research Laboratory
Cleveland, Ohio

Washington
September 1946

NATIONAL ADVISORY COMMITTEE FOR AERONAUTICS

TECHNICAL NOTE NO. 1134

DEVELOPMENT OF A PROTECTED AIR SCOOP FOR THE REDUCTION OF INDUCTION-SYSTEM ICING

By Uwe von Glahn and Clark E. Renner

SUMMARY

Aerodynamic, rain, and icing tests were conducted in the NACA icing research tunnel on the standard carburetor air scoop of a large twin-engine cargo airplane and on several under-cowling scoops designed in an effort to eliminate the characteristic ram-pressure loss accompanying impact icing of the standard scoop and the carburetor screen. Tuft and static-pressure-distribution surveys were made on the lips of the scoops and total-pressure and static-pressure readings were taken at the carburetor top deck to determine ram-pressure recovery and velocity distributions. Rates of water ingestion were determined at three simulated flight and rain conditions. Icing tests of the various scoops were made to determine the amount of duct and carburetor-screen icing.

The aerodynamic surveys indicate that an under-cowling scoop of the type investigated in these tests can achieve ram-pressure recovery comparable with that of the standard scoop. The results of the rain-ingestion tests indicate that the under-cowling-type scoop ingests less than 5 percent of the free water in the air entering the induction system as compared with the standard scoop. The icing of the carburetor screen with the under-cowling scoop was negligible; whereas with the standard scoop it was excessive.

INTRODUCTION

A large twin-engine cargo airplane was extensively used by the India-China Division, China-Burma-India Air Transport Command, to transport war material. Reports from pilots who have flown these airplanes over the India-China route during the monsoon season attribute the loss of many airplanes to induction-system icing. Instances where ice on the heated-air door prevented the pilot from using heated air have been reported. The constant use of alcohol or heated air proved not to be feasible for these conditions. Intermittent use of heated air for de-icing involves the hazard of prohibitive loss in altitude resulting from decreased engine power.

Spinner fuel injection at the entrance to the supercharger, which is standard on the engine of this cargo airplane, effectively reduces fuel-evaporation icing in the carburetor and the supercharger inlet elbow, as shown in a Pratt & Whitney Aircraft report and as demonstrated in unpublished NACA laboratory data. This induction-system icing problem is therefore limited to impact icing of the scoop, duct, screen, and carburetor-air metering parts and to throttling icing due to adiabatic expansion in the carburetor.

Elimination of free water from the induction system is an effective method of reducing the icing hazard, particularly when there is no tendency toward fuel-evaporation cooling and when parts below the carburetor are maintained at temperatures above freezing. A scoop-entrance design for preventing the entry of rain by inertia separation was proposed by Willson H. Hunter in a paper entitled "Notes on Aircraft Icing" given at the National Aeronautic meeting of the Society of Automotive Engineers at New York in March 1942 and by Kimball (reference 1). It was thought that this design could be used with little or no additional aerodynamic losses. The case of a cargo airplane operating at its service ceiling through serious icing weather warranted attempts to adapt this proposed design to the airplane in order to reduce the icing hazard in the induction system.

Aerodynamic, rain, and icing tests were conducted in the icing research tunnel of the NACA Cleveland laboratory on the standard carburetor-air scoop and several experimental scoops, which were intended to separate the rain from the air entering the scoop. The criteria selected for the design of the experimental scoops are as follows:

1. The rate of free-water ingestion must be reduced to a minimum.

2. Ram recovery must be equal to or greater than that of the standard scoop under cruising conditions above critical altitude.

3. The scoop should be automatic in its operation, requiring no attention from the pilot.

APPARATUS AND INSTRUMENTATION

The upper half of an engine cowling was installed in the 6- by 9-foot test section of the icing research tunnel. Two other center sections were modified to accommodate two experimental scoops. A rear fairing was provided back of the engine cowling to reduce the blocking effect of the model and to provide an outlet for the

simulated engine cooling air. The cowling (figs. 1 and 2) was supported by a cylindrical steel shell, which was attached to a hinged base plate 8 inches above the tunnel floor. Flight angles of attack of 0°, 4°, and 8° measured from the horizontal axis were simulated by lowering the downstream end of the base plate. A wooden dummy engine, representing the upper half of the nose section of the engine and equipped with distributors and magneto, was mounted on the base plate in proper relation to the cowling. Two orifice plates that could be remotely adjusted to obtain the desired cooling-air flow through the engine compartment were mounted behind the wooden nose section. Finned electric strip heaters were secured to the upstream orifice plate to prevent icing of the orifice openings. The orifice plates were calibrated against a standard circular orifice attached to the opening in the rear fairing of the model.

Two total-pressure rakes and a static-pressure ring (fig. 1) were located in an adapter at the junction of the inlet elbow and a water separator that replaced the carburetor. Exit ducts from the separator to both sides of the cowling completed the test induction system. Charge-air flow through the induction system was regulated by hydraulically controlled flaps located in the exit ducts. A 30-mesh screen was placed at the separator-air exits to improve the air flow in the instrumented venturi sections. Static-pressure rings and total-pressure integrating rakes in the instrumented section of the exit ducts were used to measure the charge-air mass flow. Water entering the scoop was separated from the air by four layers of parallel wires mounted at an angle to the air stream in the separator. The water was then continuously drained into two graduates. The separator was calibrated by placing a water-spray jet of known capacity inside the duct and measuring the amount of water collected at several values of airspeed and charge-air flow. This calibration showed the water separator to be at least 75-percent efficient. The duct air-stream temperature was measured by iron-constantan thermocouples installed at the carburetor top deck and instrumented sections of the exit ducts.

For each rain condition, a survey of the water concentration ahead of the scoop inlet was made with the water-sampling rake shown in figure 3. The water samples were collected in individual burettes for periods 7 to 20 minutes in duration.

DESCRIPTION OF SCOOPS

The four scoops tested were: (1) a standard carburetor-air scoop; (2) an experimental under-cowling scoop designed to protect the duct from the direct ingestion of free water; (3) a modification

of the under-cowling scoop; and (4) a combination of the standard and under-cowling scoops. The basic designs of the scoops are shown in figure 4; the scoop profiles and the typical cross-sections are shown in figure 5.

The duct of the standard scoop has a cross-sectional area of approximately 70 square inches and extends backward 52 inches to a 100° elbow leading down to the carburetor top deck. A rotary-valve-type door for admitting heated air is fitted flush with the floor of the duct ahead of the elbow. Several $\frac{1}{4}$-inch diameter holes are provided ahead of the rubber seal at the upstream end of the heated-air valve to drain the water that runs back on the duct floor. For these tests the interior of the ducts, including the side members of the heated-air valve, were sealed with sheet rubber cemented in place in order that water and air leakage would not influence the results. A vertical door, which admits filtered air and which forms the rear wall of the duct elbow, was also sealed for these tests. A removable transparent hatch was placed directly above the carburetor screen to permit observing and photographing screen ice formations. Only the forward 13.37 inches of the standard-cowling center section was altered in preparing the experimental scoops for test.

As shown in figure 5, the under-cowling scoop is designed to protect the duct inlet from the direct ingestion of free water. Water separation by the under-cowling scoop depends on the relatively great inertia of the water droplets, which causes the droplets to continue in substantially straight-line paths while the charge air curves sharply into the scoop. A theoretical analysis of the inertia-separation principle as applied to the under-cowling scoop is presented in the appendix. The front lip of the under-cowling scoop is curved downward until the leading edge coincides with the former position of the leading edge of the lower lip on the standard scoop. The rear lip is located as high and as far forward as possible to obtain the sharpest turn without reducing the inlet area.

The object in the design of the modified under-cowling scoop was to increase the radius of curvature of the inlet passage by filling in the concave rear surface of the front lip of the original under-cowling scoop. The rear lip was cut back to maintain an adequate inlet area. Because of the nature of the construction of the basic under-cowling scoop, it was impossible during the time available for these tests to alter the outer contour of the front lip as permitted by the internal changes; this change would be desirable, however, to reduce the weight of the scoop inlet and to improve the external fairing.

A scoop incorporating the features of both the standard and under-cowling scoops (fig. 5(e)) was also designed and tested. A screen was placed over the ram inlet of the standard scoop so that pressure differences caused by the icing of this screen would tend to open a door hinged a short distance back from the leading edge of the lower lip on the duct floor. The door was designed to block automatically the entire ram opening and form the outer wall of an inlet elbow of an under-cowling intake similar to the basic design tested.

SYMBOLS

The following symbols are used in the report:

H_{da} average total pressure at carburetor top deck, inches of water

H_1 total pressure of free air stream, inches of water

L cross-sectional fore-and-aft width of carburetor top deck, inches

l distance from forward wall at top deck to total-pressure-rake tubes, inches

p local static pressure on scoop surface, inches of water

p_1 test section free-stream static pressure, inches of water

S pressure coefficient $\left[1 - \left(\frac{p - p_1}{q_1}\right)\right]$

t temperature in tunnel test section, °F

V indicated airspeed, miles per hour

V_d local indicated velocity of air stream at top deck averaged for two rakes for each station value of l, feet per second

V_{da} average indicated velocity of air stream at top deck based on distribution of V_d, feet per second

V_1 indicated free-stream velocity in tunnel, feet per second

W_c charge-air flow, pounds per hour

W_e cooling-air flow, pounds per second

α angle of attack from horizontal axis, degrees

DESCRIPTION OF TESTS

Studies with wool streamers were made to determine the nature of the air flow from a region approximately 3 feet upstream of the front of the model in a vertical plane passing through the center of the model. Tuft observations for the under-cowling scoops were made from a window in the top of the tunnel test section using a mirror mounted on the model.

The test conditions for aerodynamic and simulated-rain tests are listed in the following table:

Flight condition	Approximate airspeed V (mph)	Angle of attack α (deg)	Charge-air flow W_c (lb/hr)	Cooling-air flow W_e (lb/sec) (a)
High speed	200	0	12,000	42
Cruising	160	4	7,000	26
Steep climb	160	8	12,000	42

[a]One-half of these values were used for the half-engine model.

In order to determine the aerodynamic characteristics of the scoops, pressure distributions around the scoop lips were obtained using pressure belts described in reference 2 and shown in figure 6. Total-pressure surveys made at the carburetor top deck were photographically recorded from a multitube manometer.

The free-water ingestion characteristics of the scoops were determined in simulated-rain tests with nominal water concentrations of 0, 3, 6, and 9 grams per cubic meter at the three basic flight conditions. The modified under-cowling scoop was tested only under the cruising-flight condition.

The water-droplet diameter was determined by measuring samples caught in castor oil in still air beneath the spray nozzles. Microscopic measurements of diameter were converted to drop volume and the total volume of each size range was plotted against droplet size.

The effect of the relatively few large drops was predominant in locating the peak of the curve, or "volume maximum," at 85- to 120-microns diameter for spray conditions corresponding to water concentrations of 2.0 to 11.5 grams per cubic meter, respectively. A reduction in droplet size caused by the acceleration forces in the tunnel contraction section has been observed but has not yet been quantitatively measured. The actual droplet sizes probably were smaller than indicated by measurements in still air.

Icing tests were made on the standard and under-cowling scoops for the same basic flight conditions at angles of attack of 0° and 8° and at test-section free-stream temperature of 15° and 25° F with an average water concentration of 2 to 4 grams per cubic meter. The modified under-cowling scoop was tested only at an angle of attack of 4°. Variation of water content with temperature due to freezing of some of the water in the air at 15° F may have resulted in lower icing rates but this variation could not be determined. Photographs of the scoops were taken every 2 minutes during each run, the duration of which varied from to 10 to 20 minutes; at the end of each run, the carburetor screen and the scoop entrance were photographed.

TEST RESULTS

Aerodynamic Tests

Flow studies. - Surveys around the standard scoop, made with a wool tuft, indicated flow separation from the inside of the lower lip. Wool tufts $1\frac{1}{2}$ inches long fastened on the inside of the under-cowling scoop indicated separation on the under side of the front lip and the sides of the scoop. The surface area on which separation occurred was decreased by modifying the under-cowling scoop.

Static-pressure distributions. - Pressure distributions are presented in terms of the pressure coefficient S along the scoop surfaces and are shown in figure 7 for two flight conditions used in the investigation of the standard scoop. The pressure distribution over the lips of the standard scoop shows a high negative pressure on the top surface of the upper lip with a positive pressure on the lower surface; whereas the lower-lip survey shows a positive pressure on both surfaces. The stagnation point on each lip was located near the leading edge on the lower surface. For the assumed flight conditions only slight variations in pressure distribution occurred for changes in angle of attack, charge-air

flow, and cooling-air flow. An increase in the charge-air flow from 7000 to 12,000 pounds per hour, while the angle of attack, airspeed, and proportionate cooling-air flow were maintained constant, decreased all of the pressures on the upper and the lower lips except at the stagnation points.

On the under-cowling scoop, positive pressure existed on the outer surface of the front lip near the leading edge and all along the inner surface (fig. 8(a)). The exact distribution of pressures around the leading edge of the lips is uncertain because of the $\frac{1}{2}$-inch spacing of the pressure stations. The modified under-cowling scoop was designed and tested in an effort to improve the pressure distribution of the under-cowling scoop by moving the stagnation point nearer the leading edge of the front lip. Favorable pressure gradients existed along the outer surface of the scoop and the stagnation points were at the leading edges of both lips (fig. 8(b)).

Carburetor top-deck measurements. - Typical velocity distributions across the top deck are shown in figure 9 for the standard and under-cowling scoops. Under the several test conditions for any one scoop, the velocity and the total-pressure distributions at the top deck were similar. As illustrated in figure 9, the distributions are more uniform for the under-cowling scoop than for the standard scoop, probably because flow separation occurs on the lower lip of the standard scoop and not on the lower lip of the under-cowling scoop.

The percentage total or ram-pressure recovery was calculated as $\left(1 - \frac{H_l - H_{da}}{H_l}\right) 100$, where H_{da} was obtained by integration of the total-pressure distributions shown in figure 10. By extrapolation, the under-cowling scoop had greater ram-pressure recovery at an angle of attack of 0° and a charge-air flow of 7000 pounds per hour and a considerably smaller recovery at 12,000 pounds per hour than the standard scoop for the same conditions. At an angle of attack of 4°, the ram-pressure recovery for the under-cowling scoop was slightly higher than for the standard scoop at charge-air flows below 10,000 pounds per hour but the losses were higher for the under-cowling scoop at greater air flows. Ram-pressure recoveries for the modified under-cowling scoop at these same conditions are also shown in figure 10(b). The modified under-cowling scoop demonstrated higher recovery than the other scoops at an angle of attack of 4° for the condition used in these tests. For an angle of attack of 8° (fig. 10(c)), the ram-pressure recovery for the under-cowling scoop

was considerably higher than for the standard scoop. The recovery for the scoops generally decreased with an increase in charge-air flow. The effects of angle of attack on the relative performances of the standard and under-cowling scoops are compared in figure 11 at an airspeed of 160 miles per hour for the two values of charge-air flow. The ram-pressure recovery for both scoops at angles of attack of 4° and 8° are lower for charge-air flow of 12,000 than for 7000 pounds per hour. For the standard scoop at an angle of attack of 0°, this relation is reversed and for the under-cowling scoop the ram-pressure recovery at 12,000 pounds per hour is approximately one-half that at 7000 pounds per hour.

The comparative ram-pressure recovery $\left(1 - \frac{H_1 - H_{da}}{H_1}\right) 100$ of the three scoops for the three basic flight conditions is presented in the following table:

Scoop	Angle of attack α (deg)	Approximate airspeed V (mph)	Charge-air flow W_c (lb/hr)	Cooling-air flow W_e (lb/sec)	Ram-pressure recovery (percent)
Standard	0	200	11,900	42	75.5
	4	160	7,200	26	76.0
	8	160	11,800	40	35.3
Under-cowling	0	180	12,000	42	48.3
	4	160	9,000	26	77.2
	8	160	11,600	37	63.5
Modified under-cowling	4	160	8,000	25	91.4

From aerodynamic considerations for high-speed level flight, the standard scoop is more satisfactory than the under-cowling scoop. For steep climb at sea level or cruise at ceiling conditions, the under-cowling scoop has greater ram-pressure recovery than the standard scoop. Furthermore, the ram-pressure recovery for the modified under-cowling scoop at cruising conditions is higher than for either of the other scoops. The aerodynamic performance of the modified under-cowling scoop based on the results obtained at an angle of attack of 4° will probably compare favorably with the standard scoop for high-speed level flight and be still better for climb conditions.

Rain Tests

The scoops were tested under rain conditions that actually varied from an average free-water concentration of 2.0 to 11.5 grams per cubic meter. As shown in figure 12, large amounts of water were ingested by the standard scoop in direct proportion to the free water in the air stream for the three basic flight conditions. The modified under-cowling scoop ingested about 5 percent of the water collected by the standard scoop. No measurable amount of water was collected with the under-cowling scoop, which indicates its excellent inertia separating qualities.

Characteristic spray profile distributions in relation to the standard and under-cowling type scoops are shown in figure 13. The effective drop size obtained during these tests was probably larger than exists in most clouds but considerably smaller than rain drops.

Icing Tests

Typical locations and profiles of the ice formations on each of the scoops for similar test conditions are shown in figure 14.

Standard scoop at 25° F. - Heavy accumulations of slushy glaze ice formed on the inlet lips of the standard scoop at a test-section temperature of 25° F (fig. 15). Heavy formations occurred in the duct with a thickness of as much as 1.25 inches along the ceiling and floor of the duct as far back as the elbow. High ridges of ice collected at the top surface of the lower lip and icing of the carburetor screen occurred under all conditions. Ice always formed first on the rear and the sides of the screen, gradually closing the screen opening until only a small portion on the forward side remained open. At an increased angle of attack, more ice formed on the ceiling of the duct due to the greater area directly exposed to water-droplet impingement. The required air flow through the carburetor duct was maintained as long as possible by gradually opening the charge-air outlet flaps. Severe impact icing up to 1 inch thick formed on the filtered-air door.

Standard scoop at 15° F. - As shown in figure 16, heavy rime ice formed on the lips of the standard scoop at 15° F. Ice formed up to 0.25 inch thick on the inside of the duct as far back as the elbow increasing in severity with an increase in angle of attack. Impact ice formed on the filtered-air door to a thickness of 0.25

to 0.37 inch. Some icing was observed on the carburetor screen. Photographs (fig. 17) showing the progressive formation of ice on the scoop were taken at 2-minute intervals through a tunnel observation window.

Under-cowling scoop at 25° F. - When the under-cowling scoop was tested under the same conditions as the standard scoop, heavy clear ice accumulated on the outer surface of the front lip at a temperature of 25° F, as shown in figure 18. The first 6 to 8 inches from the leading edge on the inner surface of the front lip were free of ice under all test conditions. From this point rearward, medium deposits of ice collected as far as the first access hatch. At times ice accumulations were observed for a short distance, occurring as a result of secondary inertia separation of the residual water droplets as the air turned into the horizontal part of the duct. As the angle of attack is increased, the curvature for inertia separation of water is reduced, exposing more of the duct ceiling to water impingement. Slightly larger areas of duct icing occurred as the angle of attack of the model was increased. No ice formed on the filtered-air door, heated-air door, carburetor screen, or floor of the duct. Ice formed on the under surface of the rear lip of the scoop to a thickness of 0.75 inch during a 20-minute run.

Under-cowling scoop at 15° F. - As shown in figure 19, a medium deposit of rime ice formed on the outside of the under-cowling scoop and on the under side of the rear lip to a maximum thickness of 0.06 inch at a temperature of 15° F. A thin layer of ice formed 6 to 8 inches back of the leading edge on the inside of the front lip, as in the tests at 25° F, but this deposit was rarely more than 0.06 inch thick and was thin enough to permit the laminations of the wooden scoop to be visible. No ice formed on the filtered-air door, heated-air door, or on the carburetor screen.

The rate of ice formation on the under-cowling scoop is indicated by the series of photographs presented in figure 20.

Modified under-cowling scoop. - The modified under-cowling scoop experienced the same general exterior icing as the under-cowling scoop; some impact ice formed on the screen and the filtered-air door, as shown in figure 21. The icing of the screen was anticipated because some water had been collected in the water separator during the rain tests. Light to moderate ice formations were observed in the ducts at the same general areas as with the under-cowling scoop.

Combined standard and under-cowling scoop. - Icing tests were conducted on the combined standard and under-cowling scoop with a 4-mesh screen placed over the ram inlet. Because the inlet screen must become plugged with ice before the door will open fully, this scoop did not provide effective inertia separation until the screen was fully iced. Consequently, this scoop under icing conditions permitted a considerable amount of ice to form on the carburetor screen and heavy duct icing was noted. The amount of icing of the carburetor screen varied with the degree and rate of opening of the under-cowling door; hence, with the icing rate of the scoop-entrance screen. A 16-mesh entrance screen gave improved performance in icing conditions, as shown in figure 22, but at the expense of increased aerodynamic losses in nonicing conditions.

DEVIATIONS FROM TRUE FLIGHT CONDITIONS

The simulated conditions in the icing research tunnel for the tests of the scoops differed from true flight conditions because of the nature of the setup and the tunnel characteristics. The main deviations are:

1. The tests were conducted without benefit of engine heat, which in true flight conditions may tend to decrease some of the carburetor-duct icing.

2. The ram-pressure-recovery and water-ingestion measurements obtained in the tests may be too high for all the scoops owing to the sealing of drain holes and other openings in the carburetor duct.

3. The tests were run without the presence of the propeller and no corrections were made for the wind-tunnel wall interference on the flow field. The comparative results are believed to be valid, however, because the scoops were tested under substantially the same conditions.

4. With the spray equipment used in these tests, true cloud icing conditions were not simulated in the tunnel. In most impact-icing conditions, cloud-droplet diameters vary between 10 and 30 microns and the water content varies between 0.5 and 1.5 grams per cubic meter. The size of the drops in freezing mist and drizzle varies between 50 and 400 microns, whereas freezing rain drops can attain a size of 2000 microns. Hence, the droplet sizes used in the tunnel were intermediate between those of cloud and rain.

SUMMARY OF RESULTS

The principal results of aerodynamic, rain, and icing tests of the standard and under-cowling type scoop designs in the icing research tunnel for angles of attack of 0° to 8° and charge-air flows of 7000 and 12,000 pounds per hour with corresponding cooling-air flows of 26 and 42 pounds per second may be summarized as follows:

Aerodynamic Tests

1. At all angles of attack, the under-cowling-type scoops had greater ram-pressure recovery than the standard scoop for charge-air flows corresponding to cruising conditions.

2. At charge-air flows corresponding to climb conditions and at an airspeed of 160 miles per hour, the under-cowling scoop had less ram-pressure recovery at angles of attack of 0° and 4° than the standard scoop but greater recovery at 8°.

3. At an angle of attack of 4°, the modified under-cowling scoop had greater ram-pressure recovery than the other scoops up to charge-air flows corresponding to climb.

4. At an angle of attack of 4° and cruising charge-air flows, the under-cowling-type scoops gave improved velocity distributions at the carburetor top deck as compared with those of the standard scoop.

Rain Tests

5. The rate of water ingestion of the standard scoop increased in direct proportion to the free water in the air and was higher than for the other scoops.

6. The rate of water ingestion by the under-cowling scoop was too small to be measured with the available equipment.

7. At an angle of attack of 4°, the modified under-cowling scoop ingested water at a rate approximately 5 percent of that of the standard scoop under the same conditions.

Icing Tests

8. Heavy duct and carburetor-screen icing occurred with the standard scoop at 25° F at all angles of attack; at 15° F, moderate duct and light screen icing were observed.

9. Light to moderate duct icing and no carburetor-screen icing occurred with the under-cowling scoop at temperatures of 15° and 25° F at all angles of attack.

10. Light to moderate duct icing and traces of screen icing were observed on the modified under-cowling scoop at an angle of attack of 4° at a temperature of 25° F; whereas at a temperature of 15° F, no screen ice and only light duct ice were observed.

Aircraft Engine Research Laboratory,
National Advisory Committee for Aeronautics,
Cleveland, Ohio, June 21, 1946.

APPENDIX - CALCULATION OF DROPLET THEORETICAL PATHS

In order to demonstrate analytically the inertia-separation principle of the under-cowling scoop, a hypothetical field of two-dimensional potential flow was selected to represent approximately the flow ahead of the engine cowling and the paths of 15- and 40-micron diameter droplets were calculated and plotted. The streamline paths selected were rectangular hyperbolas of the type represented by the general equation

$$\psi = -xy = k$$

where x and y are the axes, k is an arbitrary constant, and ψ is the stream function. The cross-sectional outline of the under-cowling scoop was superimposed on the field of flow in an arbitrary position selected to illustrate as clearly as possible the inertia-separation principle involved.

The method used to calculate the droplet paths is outlined in reference 3 and is based on the following assumptions:

1. The individual droplets were assumed to be traveling on particular streamlines with a free-stream velocity of 300 feet per second at a distance 4 feet ahead of the engine cowling.

2. The speed of the droplet was assumed to remain constant at a free-stream velocity of 300 feet per second in a direction tangent to the original streamline at all points.

3. The radius of curvature of the original streamline was always used in determining the centrifugal acceleration on the droplet even though the droplet path had deviated considerably from the original streamline.

4. Stokes' law was assumed to be valid at these values of droplet Reynolds number.

The normal velocity of the droplets was calculated from Stokes' law by

$$u = \frac{2}{9} \frac{r^2 v^2}{\mu \rho}$$

where

u component of droplet local velocity normal to original streamline, ft/sec

r droplet radius, ft

v droplet velocity, ft/sec

μ absolute air viscosity, lb-sec/sq ft

ρ streamline radius of curvature, ft

The droplet deviation is then found from the equation

$$\delta = \int_{t_A}^{t_B} u\,dt$$

where

δ deviation of droplet normal to streamline, ft

t time, sec

Subscripts A and B represent the limits of the increment.

In order to show the effect of drop size, the paths of droplets of 15- and 40-micron diameter were plotted as shown in figure 23. As indicated by these paths, only the small droplets enter the scoop. Evidence of the entrance of small droplets into the under-cowling scoops was found in the presence of light to moderate ice accretions on the inside upper surface of the inlet duct and in the small amount of water ingested by the modified under-cowling scoop. On the basis of work done by Dr. Irving Langmuir of the General Electric Co. on the paths of water droplets at values of droplet Reynolds number beyond the range of validity of Stokes' law, it is estimated that the 15- and 40-micron droplet paths as calculated from Stokes' law may correspond to the true paths of droplets whose diameters are approximately twice these values. Because the measured average droplet diameter by volume maximum in these tests was between 85 and 120 microns, the droplet paths shown in figure 23(b) probably represent true paths for the conditions of the tests.

REFERENCES

1. Kimball, Leo B.: Icing Tests of Aircraft-Engine Induction Systems. NACA ARR, Jan. 1943.

2. Corson, Blake W., Jr.: The Belt Method for Measuring Pressure Distribution. NACA RB, Feb. 1943.

3. Stickley, A. R.: Some Remarks on the Physical Aspects of the Aircraft Icing Problem. Jour. Aero. Sci., vol. 5, no. 11, Sept. 1938, pp. 442-446.

214+748

A Maintenance hatches
B Observation hatch
C Heated-air door
D Filtered-air door
E Standard scoop entrance
F Cowling-support shell
G Dummy engine
H Upstream static-pressure ring plane
I Adjustable orifice plates
J Downstream static-pressure ring plane
K Top deck total-pressure rakes and static-pressure ring plane
L Tail cone
M Water inertia separator
N Side plates $\alpha = 0^\circ$
O 30-mesh screen
P Plane of integrating total-pressure rake and static-pressure ring
Q Carburetor screen

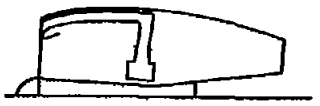

NATIONAL ADVISORY
COMMITTEE FOR AERONAUTICS

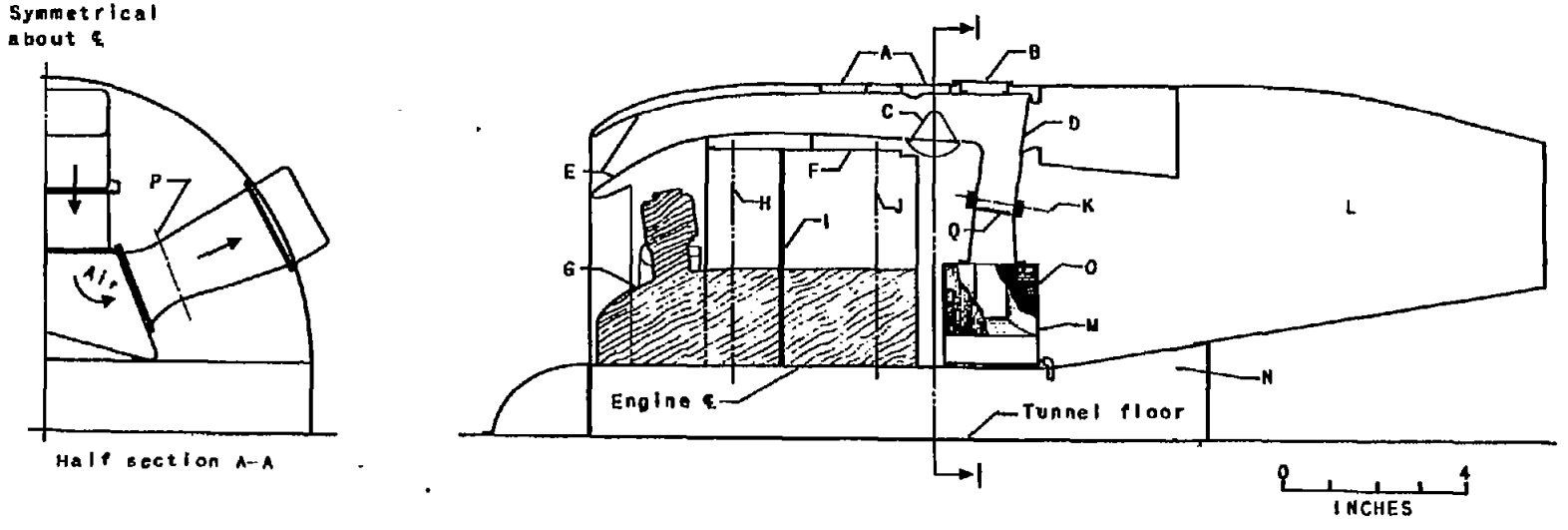

Figure 1. - Schematic diagram of induction-system installation with standard scoop. $\alpha = 0^\circ$, 4°, and 8°.

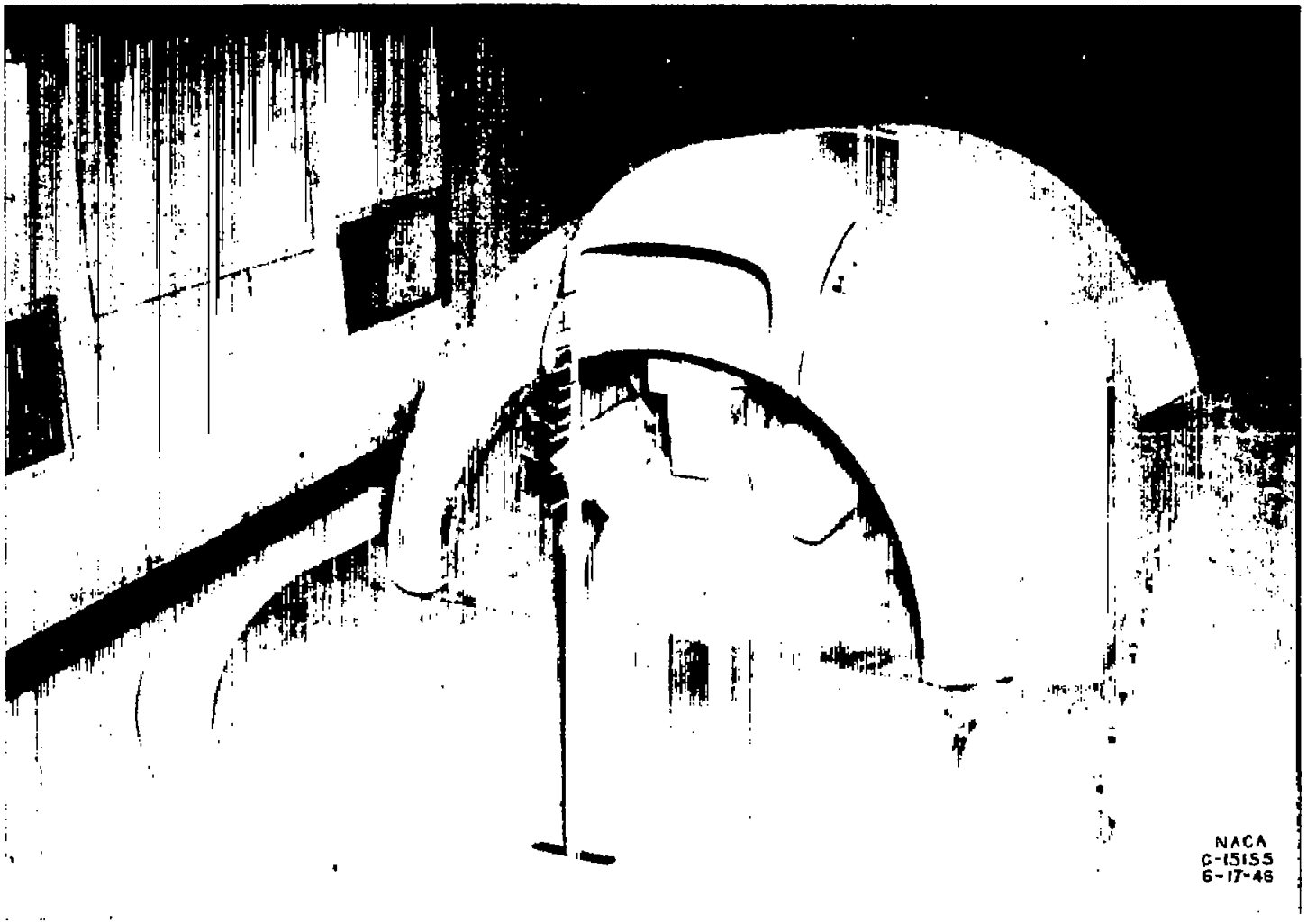

Figure 2. - Installation of induction-system test setup in icing research tunnel.

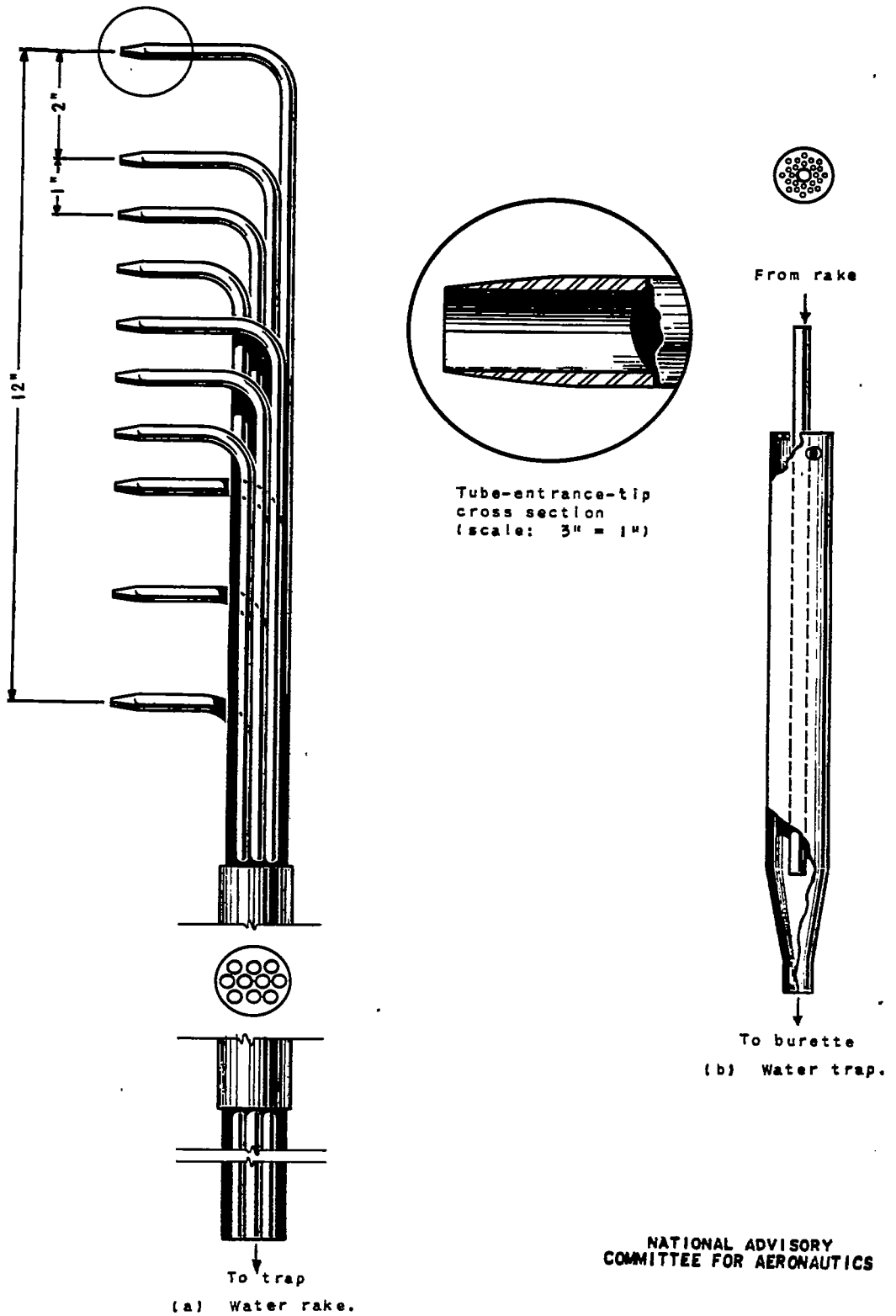

Figure 3. - Free-water sampling rake and water trap.

(a) Standard scoop.

(b) Under-cowling scoop.

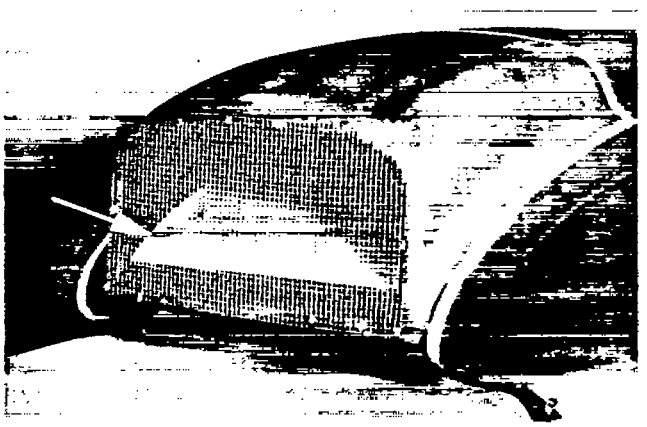

NACA
C-11955
8-17-45

(c) Combination of standard and under-cowling scoops. (Arrow shows inlet door.)

Figure 4. - Basic design of standard and under-cowling scoops.

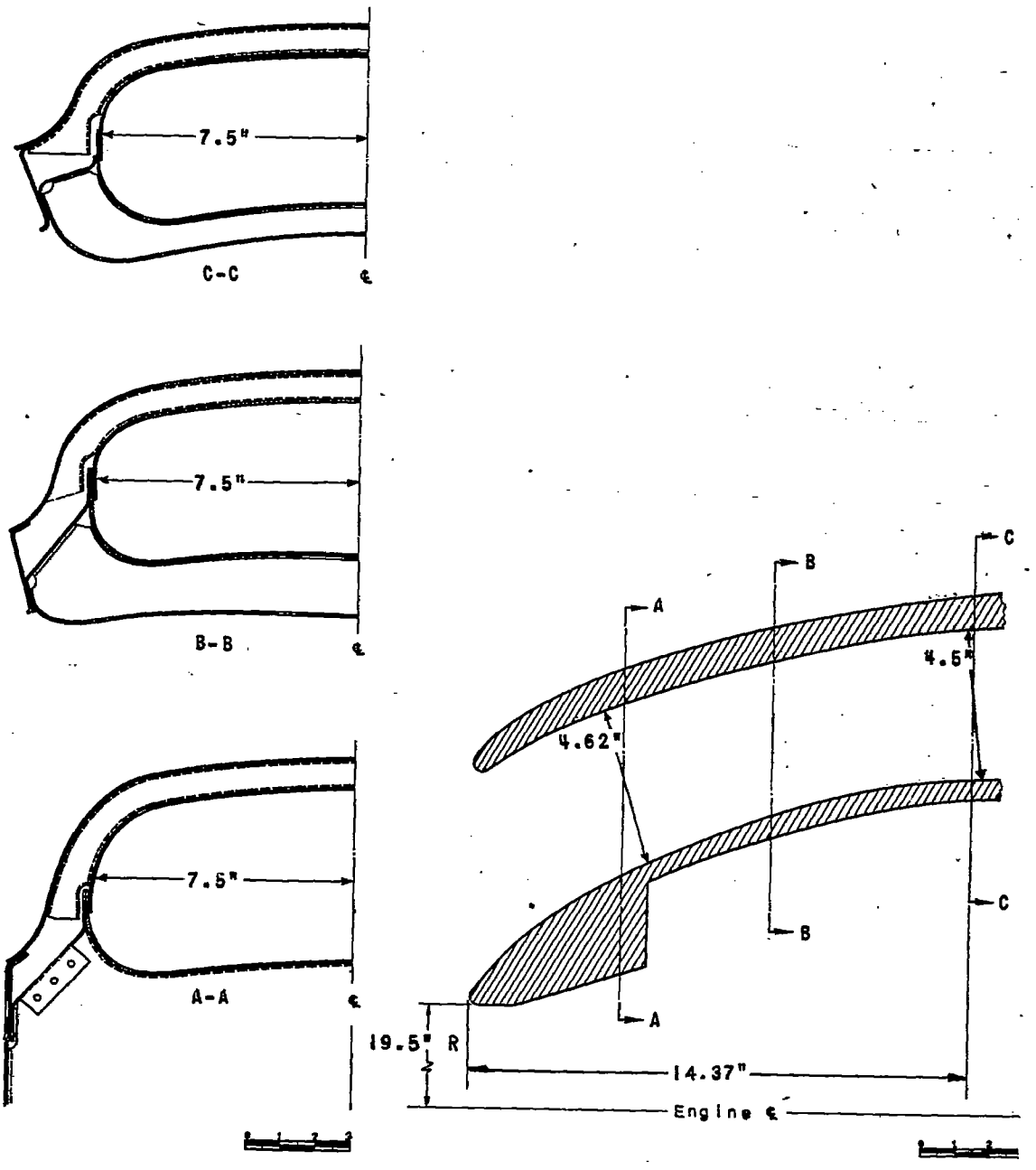

(a) Standard scoop.

Figure 5. - Profiles and typical cross sections of standard scoop, under-cowling scoop, modified under-cowling scoop, and combination of standard and under-cowling scoops.

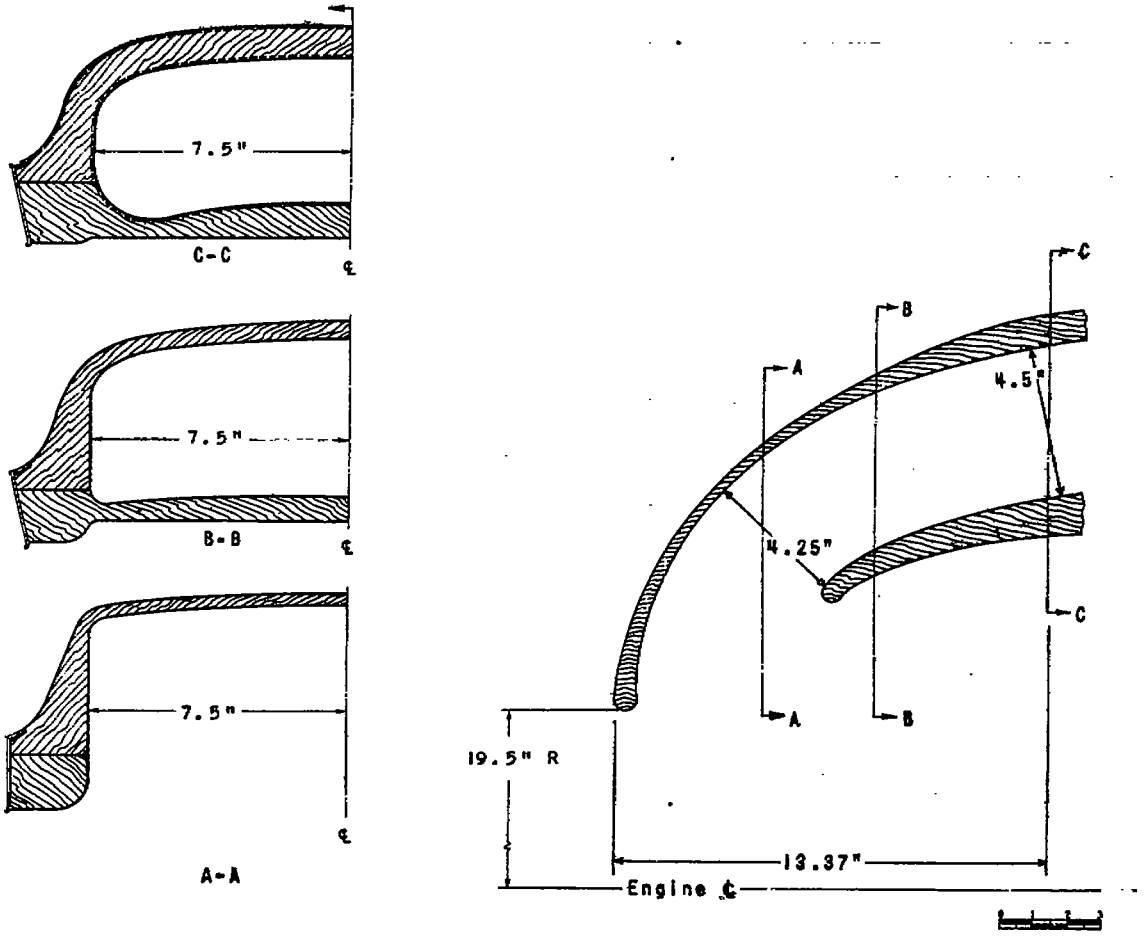

(b) Under-cowling scoop.

NATIONAL ADVISORY COMMITTEE FOR AERONAUTICS

Figure 5. - Continued. Profiles and typical cross sections of standard scoop, under-cowling scoop, modified under-cowling scoop, and combination of standard and under cowling scoops.

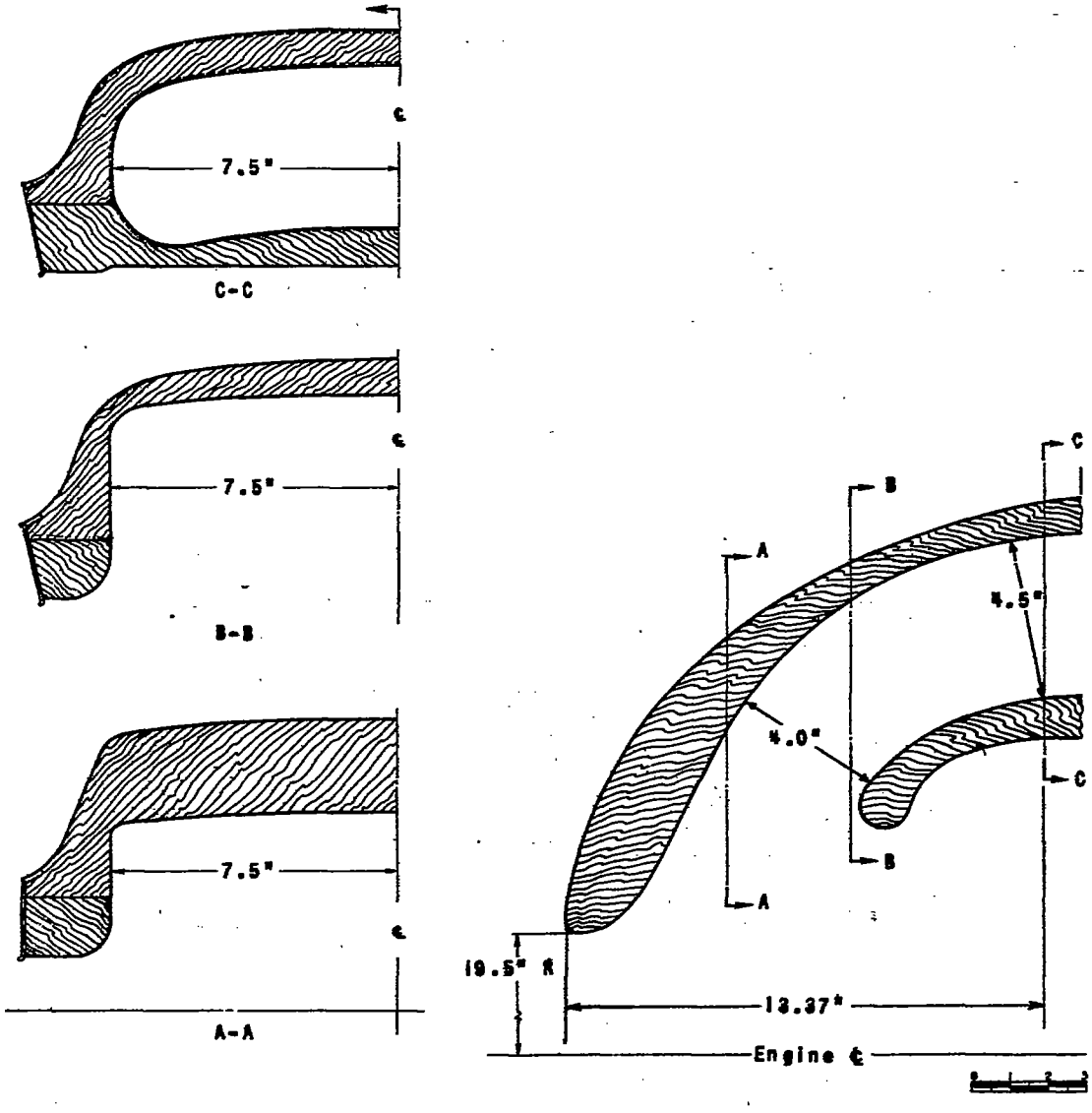

(c) Modified under-cowling scoop.

NATIONAL ADVISORY
COMMITTEE FOR AERONAUTICS

Figure 5. - Continued. Profiles and typical cross sections of standard scoop, under-cowling scoop, modified under-cowling scoop, and combination of standard and under-cowling scoops.

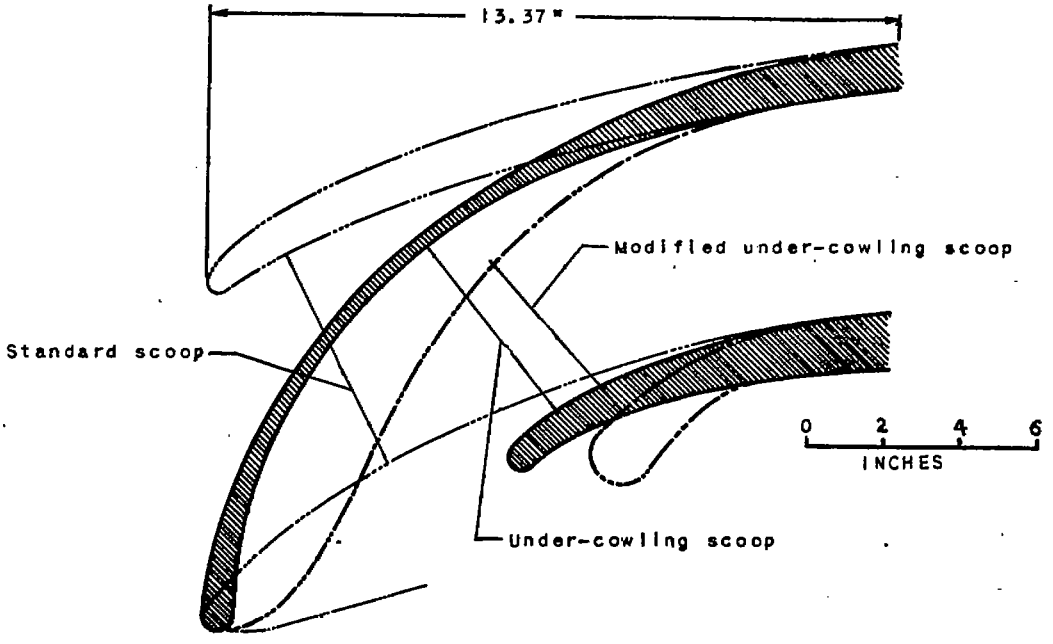

(d) Under-cowling type scoops superimposed on standard scoop.

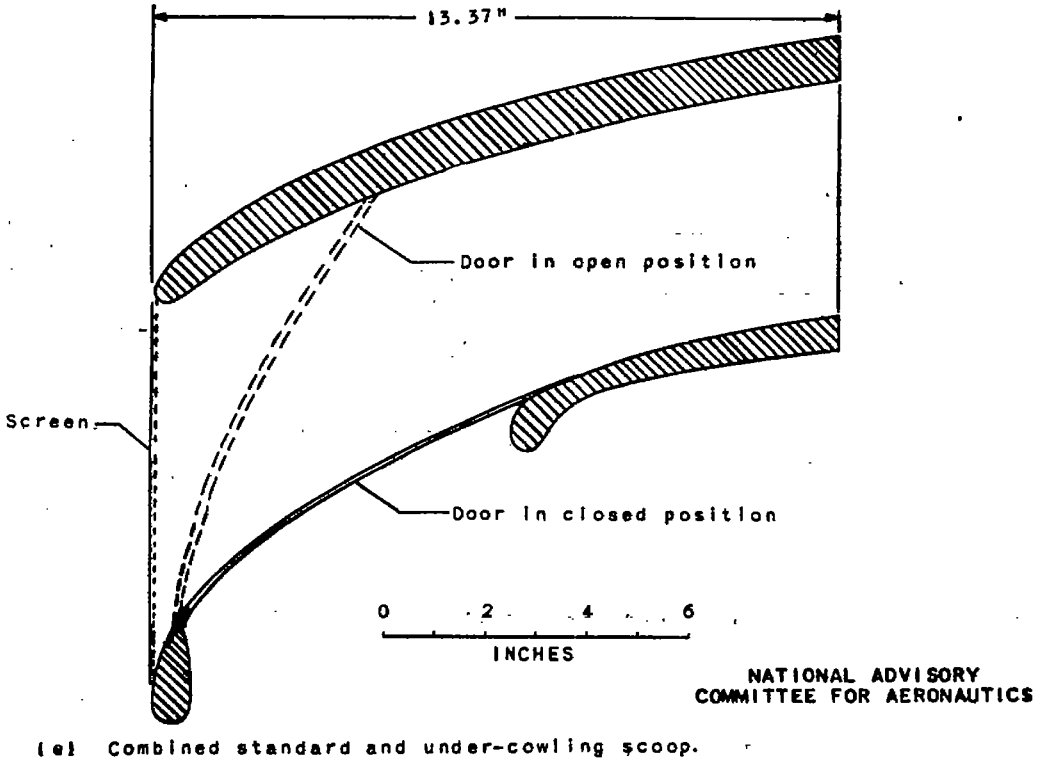

(e) Combined standard and under-cowling scoop.

Figure 5. - Concluded. Profiles and typical cross sections of standard scoop, under-cowling scoop, modified under-cowling scoop, and combination of standard and under-cowling scoops.

Figure 6. - Pressure-belt installation used in pressure-distribution survey.

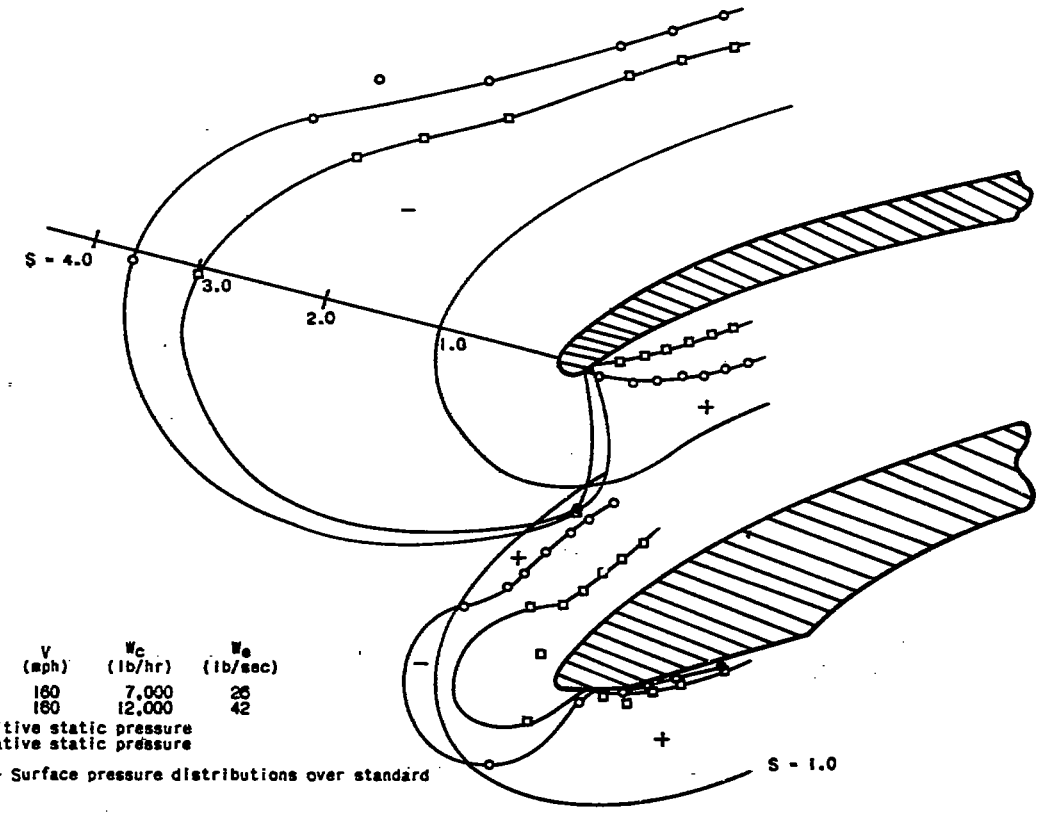

Figure 7. - Surface pressure distributions over standard scoop.

NATIONAL ADVISORY
COMMITTEE FOR AERONAUTICS

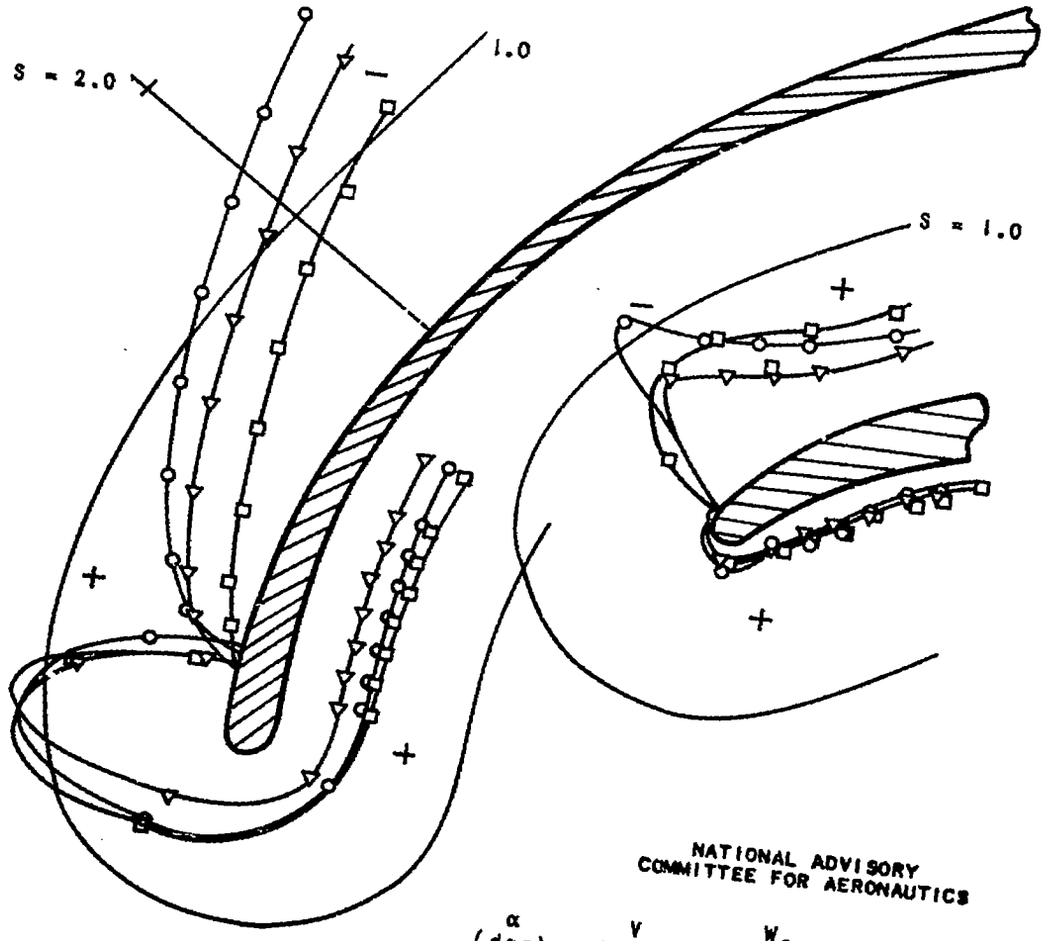

α (deg)	V (mph)	W_c (lb/hr)	W_e (lb/sec)
□ 0	180	12,000	42
▽ 4	160	7,000	26
○ 8	160	12,000	42

+ Positive static pressure
− Negative static pressure

(a) Under-cowling scoop.

Figure 8. - Surface pressure distributions over under-cowling scoop and its modification.

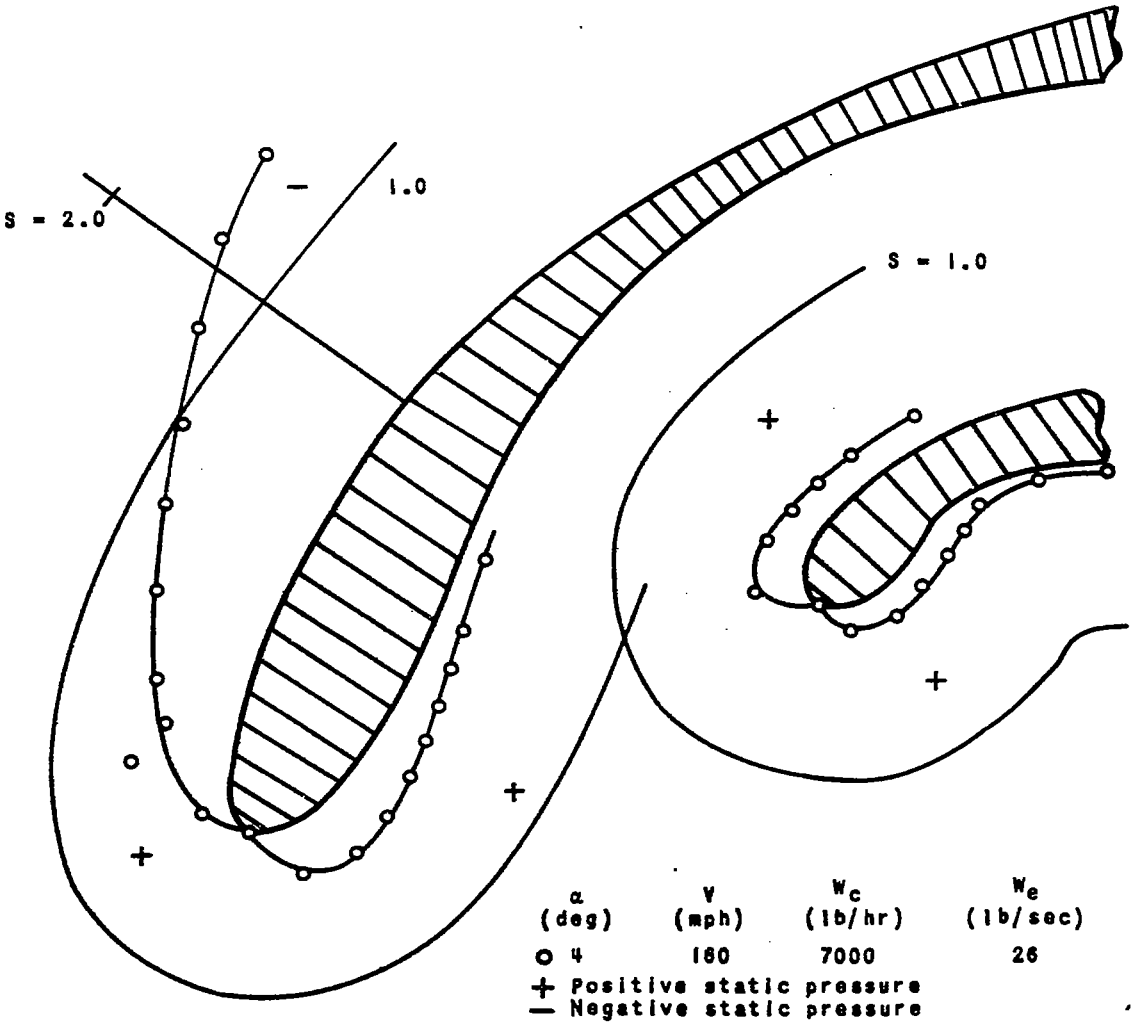

(b) Modified under-cowling scoop.

NATIONAL ADVISORY COMMITTEE FOR AERONAUTICS

Figure 8. - Concluded. Surface pressure distributions over under-cowling scoop and its modification.

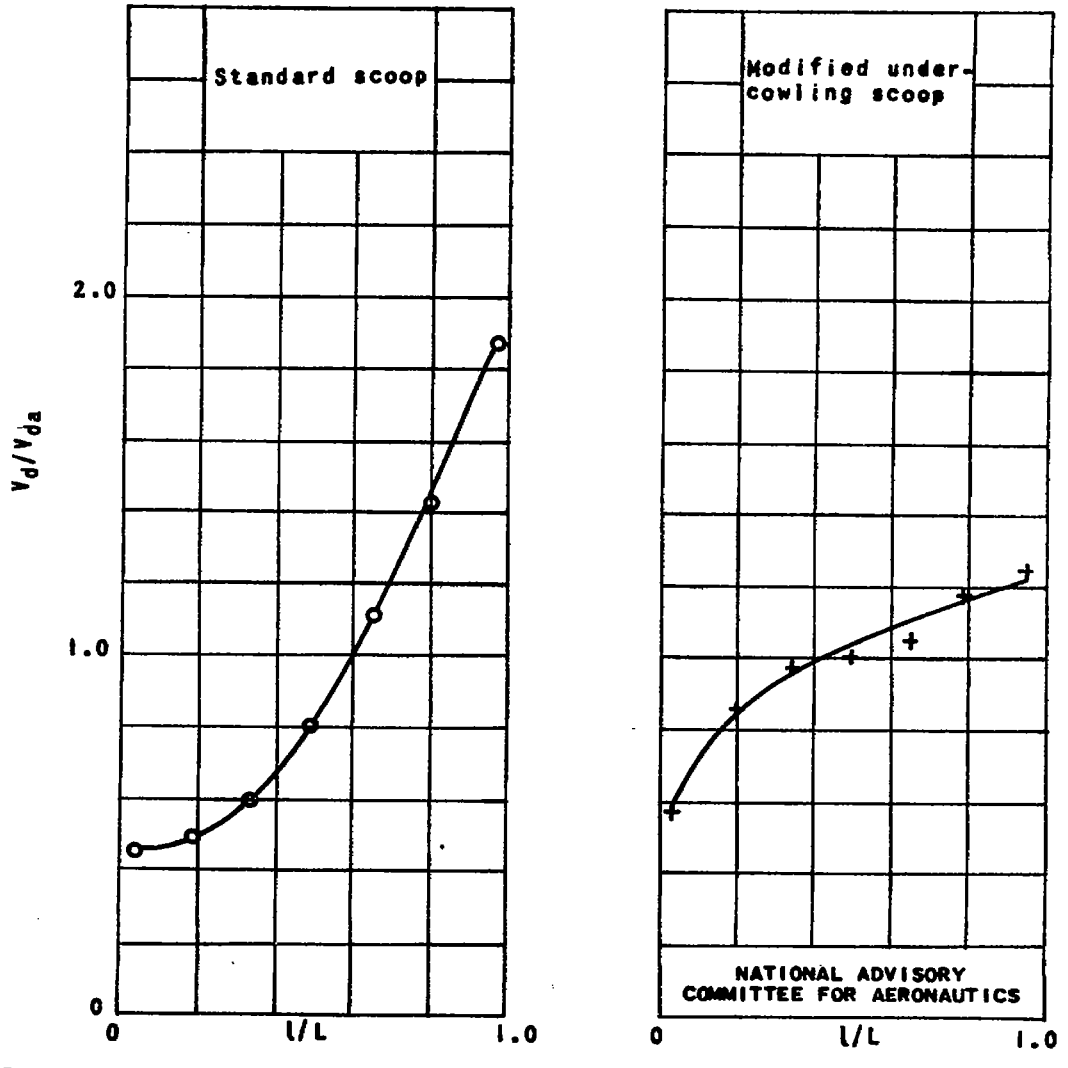

Figure 9. - Typical velocity distributions for the standard and modified under-cowling scoops at carburetor top deck. α, 4°; V, 160 miles per hour; W_c, 12,000 pounds per hour.

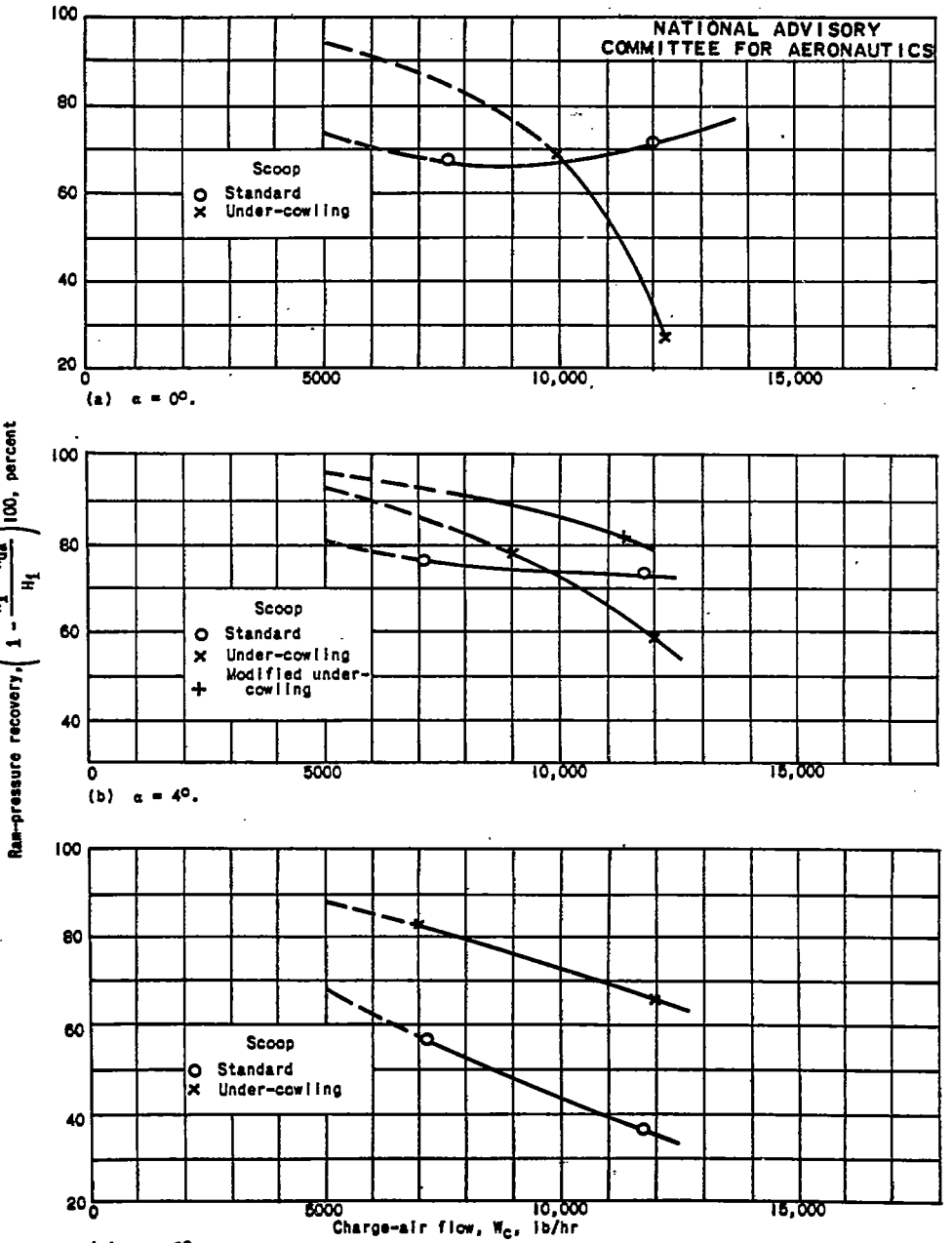

(a) $\alpha = 0°$.

(b) $\alpha = 4°$.

(c) $\alpha = 8°$.

Figure 10.- Variation of ram-pressure recovery with charge-air flow for three scoops. V, 160 miles per hour.

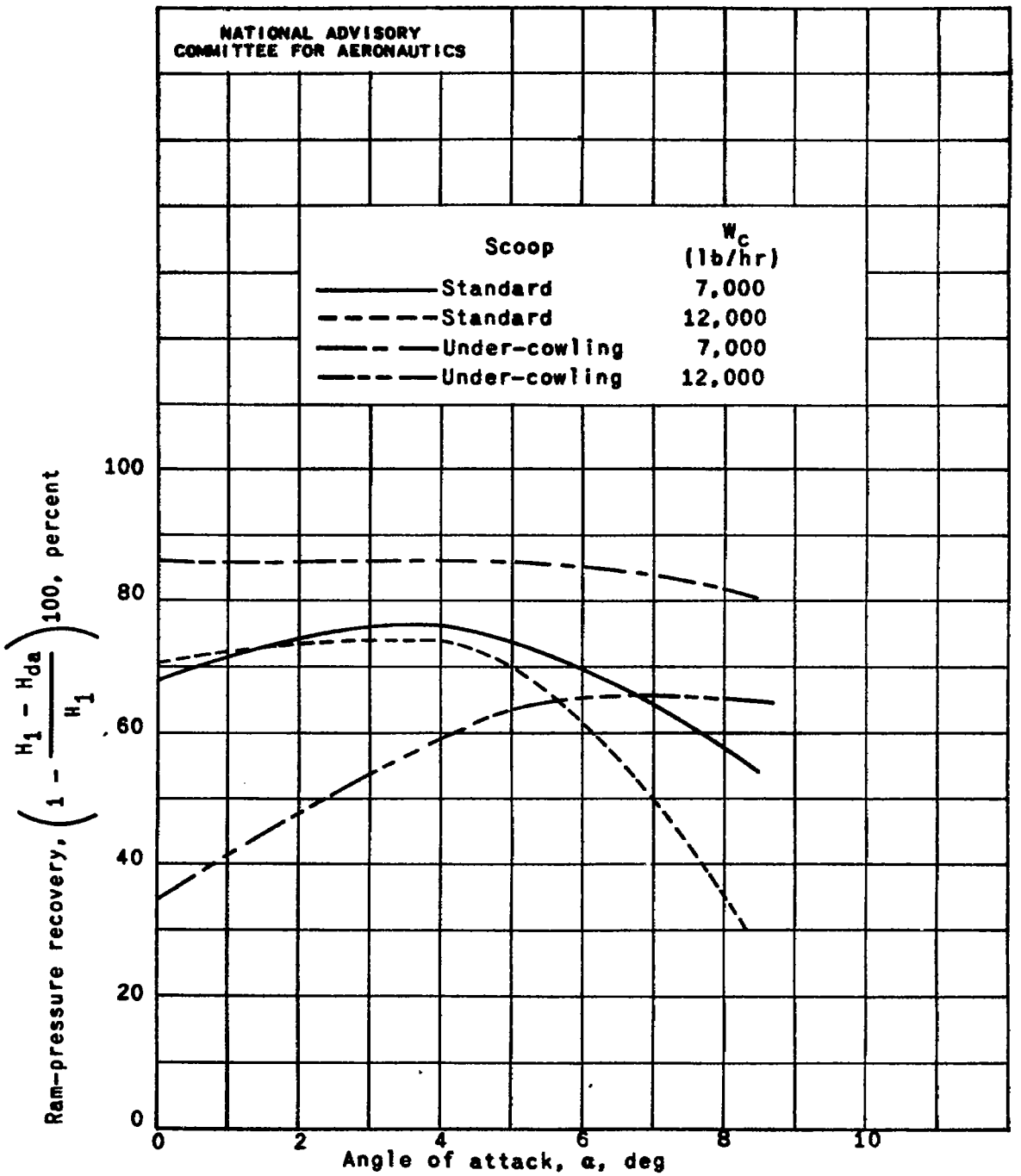

Figure 11.- The effect of change in angle of attack on ram-pressure recovery for standard and under-cowling scoops. V, 160 miles per hour.

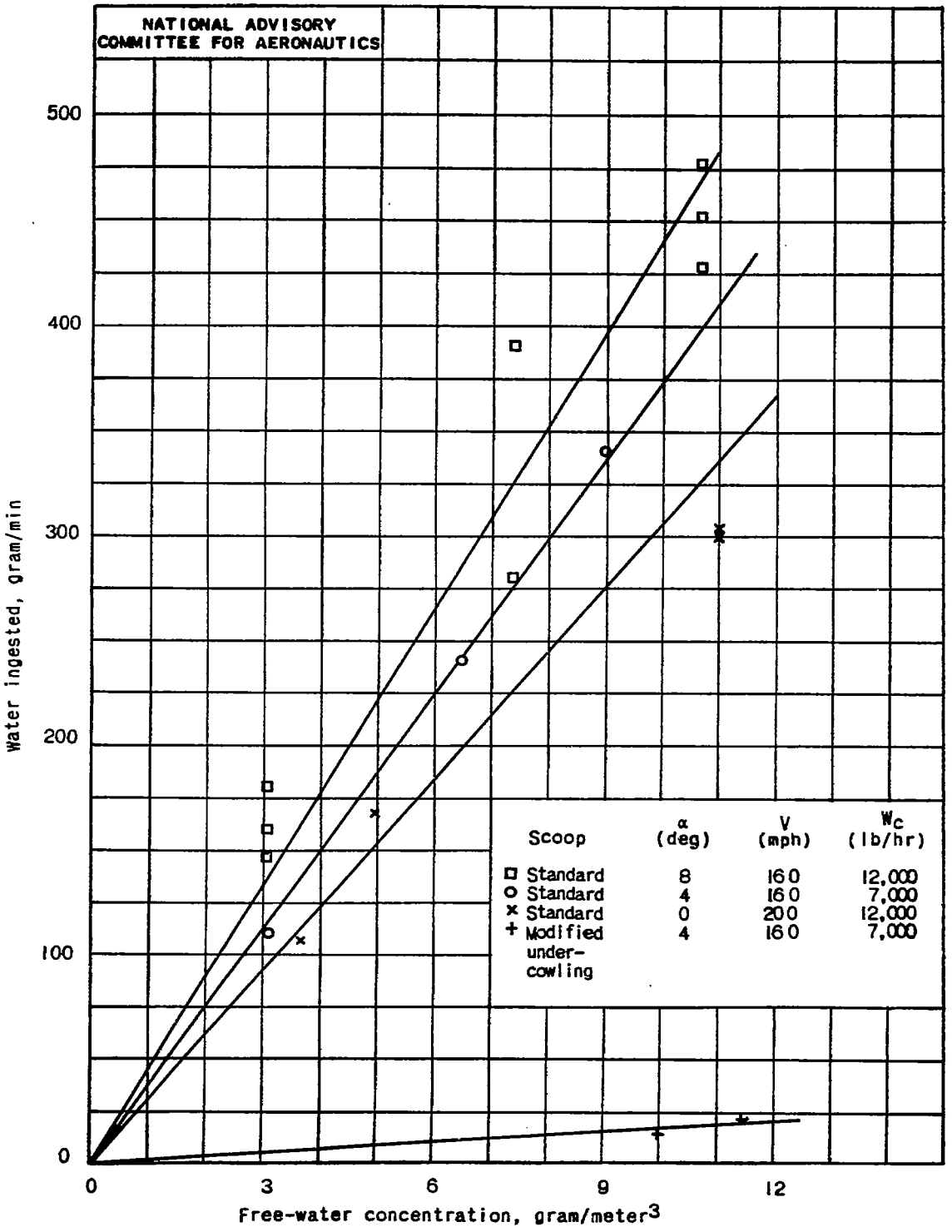

Figure 12. - Relation between free-water content and rate of water ingestion in standard and modified under-cowling scoops.

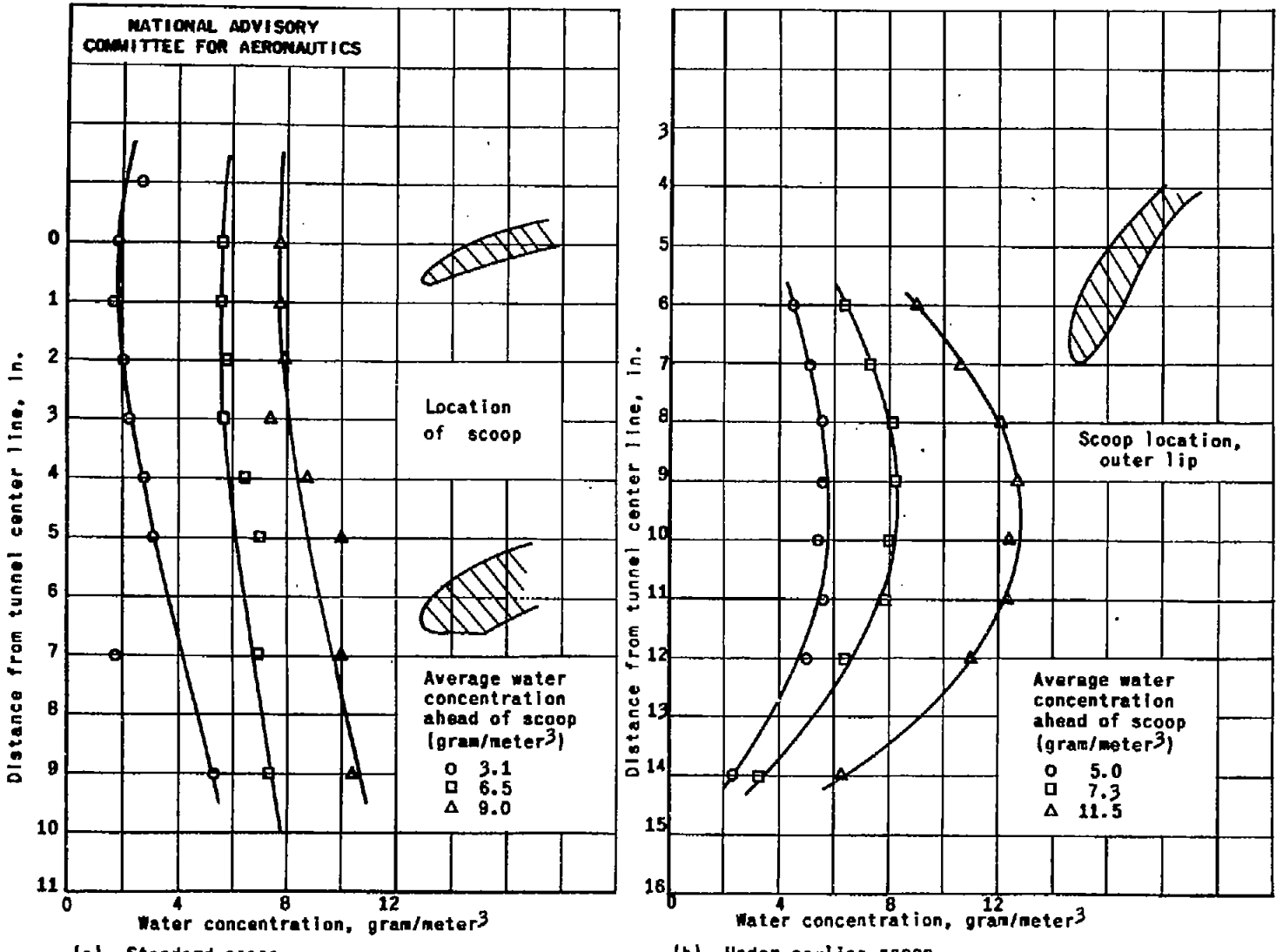

(a) Standard scoop.

(b) Under-cowling scoop.

Figure 13.- Typical spray profiles 17 inches ahead of standard and under-cowling type scoops. α, 4°; V, 160 miles per hour; W_c, 7000 pounds per hour.

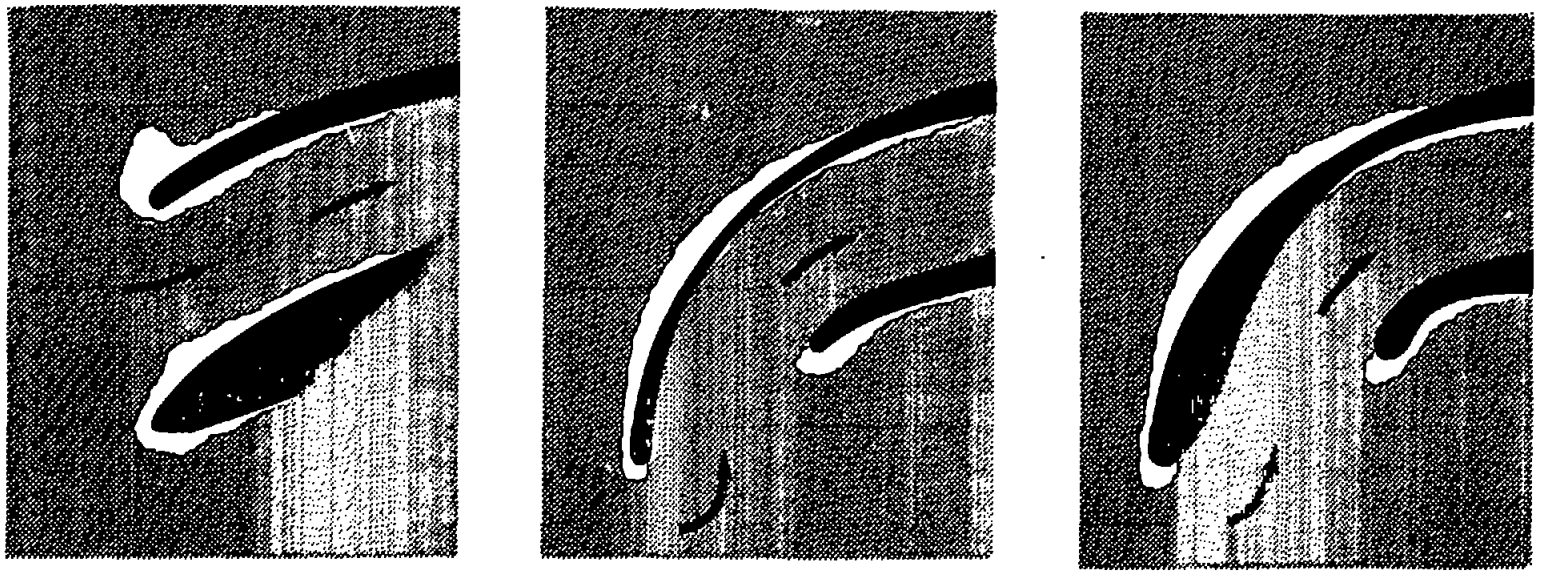

(a) Standard scoop.

(b) Under-cowling scoop.

(c) Modified under-cowling scoop.

NATIONAL ADVISORY
COMMITTEE FOR AERONAUTICS

Figure 14. - Cross sections of scoops showing typical ice formations.

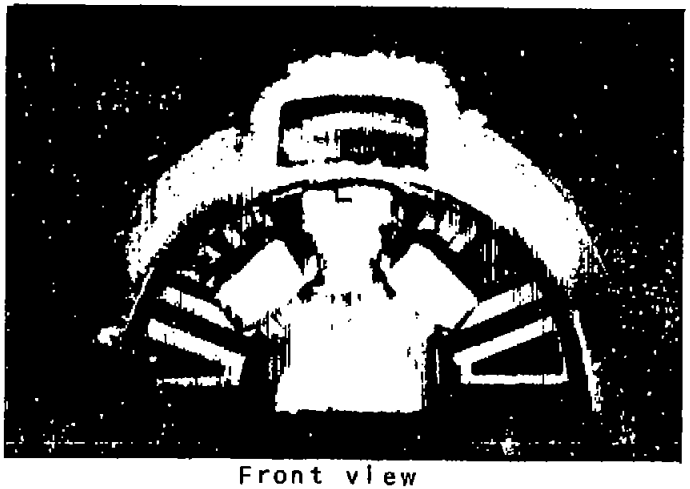

Front view

Three-quarter view

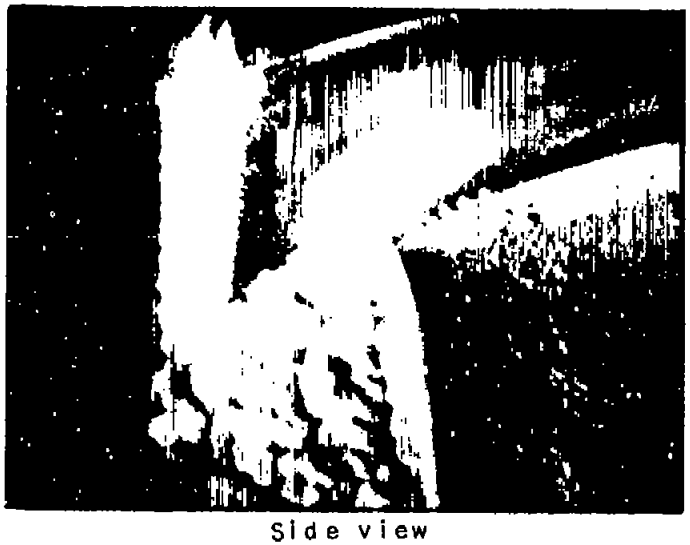

Side view

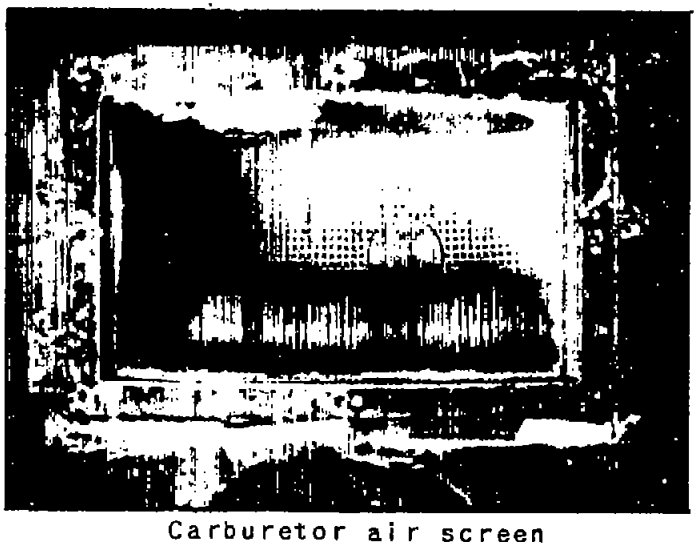

Carburetor air screen

(a) α, 8°; V, 160 miles per hour.

NACA
C-10051
5-16-45

Figure 15. - Glaze-ice formations on standard scoop after 15-minute run. t, 25° F; W_c, 12,000 pounds per hour; W_e, 42 pounds per second.

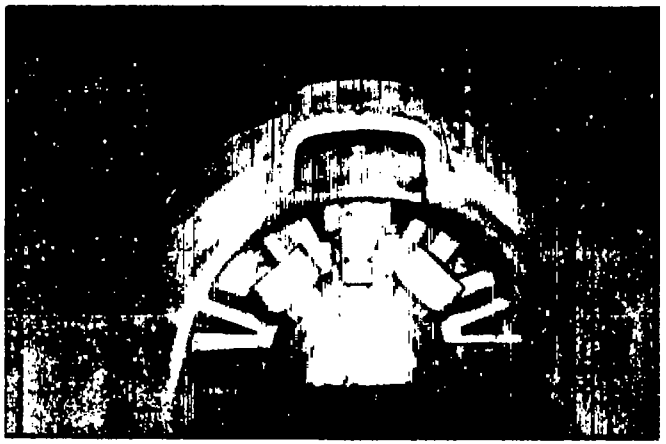

Front view

Three-quarter view

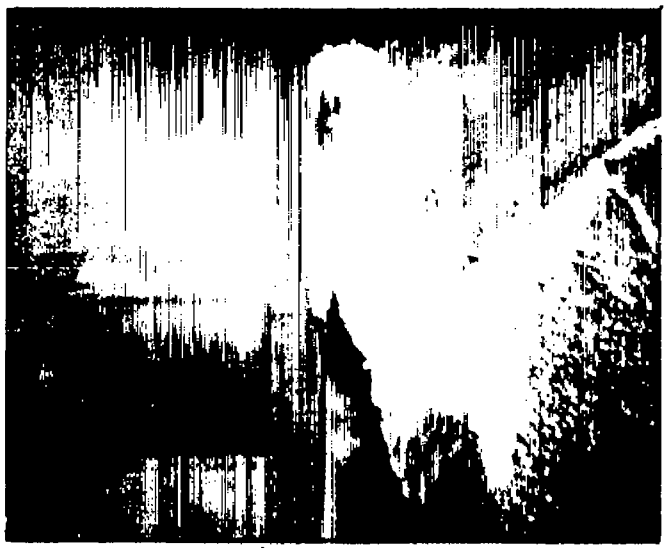

Side view

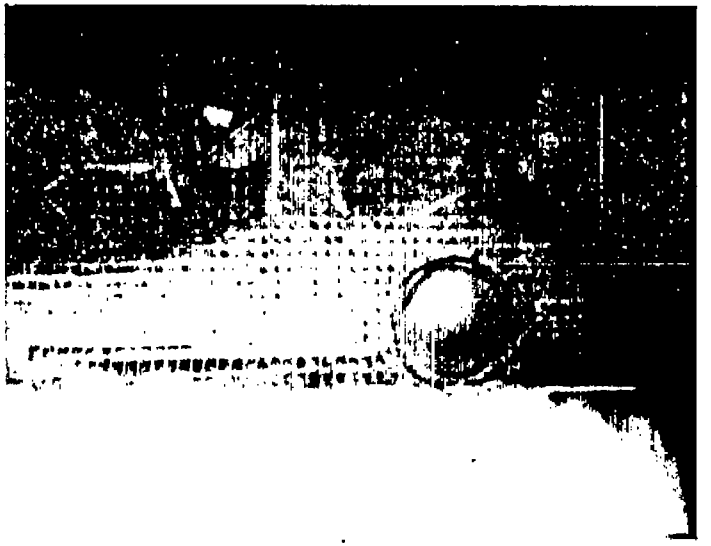

Carburetor air screen

(b) α, 0°; V, 200 miles per hour.

NACA
C-10052
5-16-45

Figure 15. - Concluded. Glaze-ice formations on standard scoop after 15-minute run. t, 25° F; W_c, 12,000 pounds per hour; W_e, 42 pounds per second.

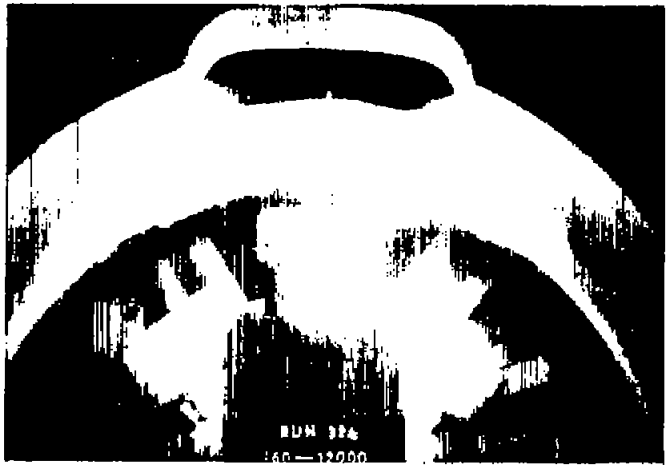

Front view

Side view

Three-quarter view

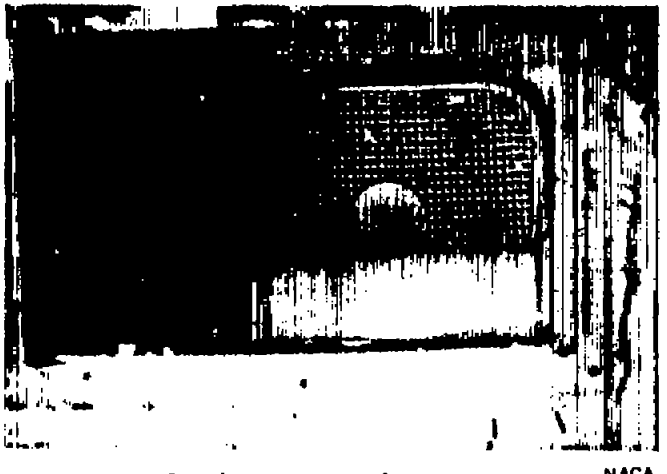

Carburetor air screen

NACA
C-10053
5-16-45

(a) α, 8°; V, 160 miles per hour; 25-minute run.

Figure 16. - Rime-ice formations on standard scoop. t, 15° F; W_c, 12,000 pounds per hour; W_e, 42 pounds per second.

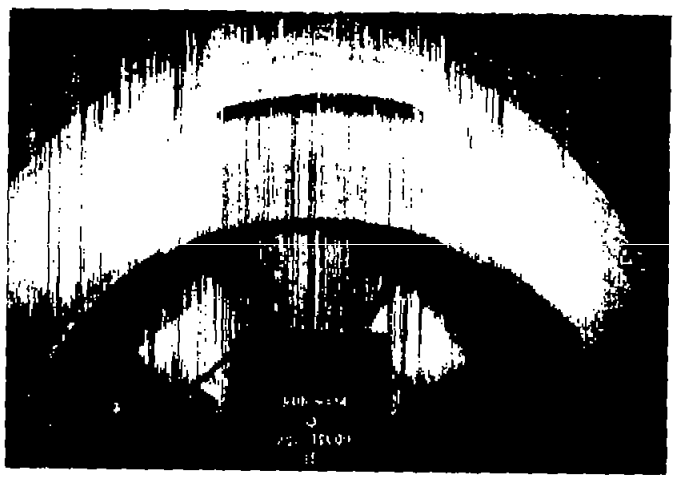

Front view

Side view

Three-quarter view

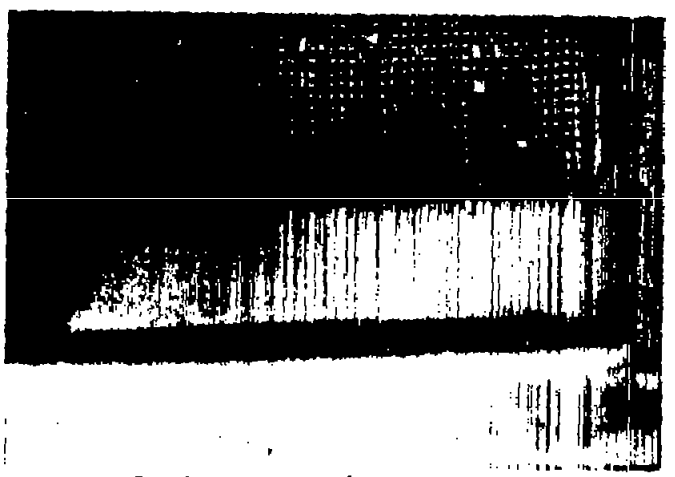

Carburetor air screen

NACA
C-10054
5-16-45

(b) α, 0°; V, 200 miles per hour; 12-minute run.

Figure 16. - Concluded. Rime-ice formations on standard scoop. t, 15° F; W_c, 12,000 pounds per hour; W_e, 42 pounds per second.

2 minutes

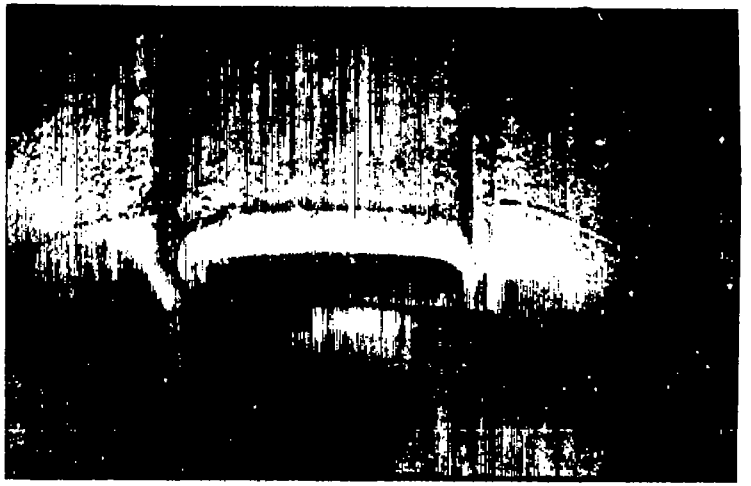

4 minutes

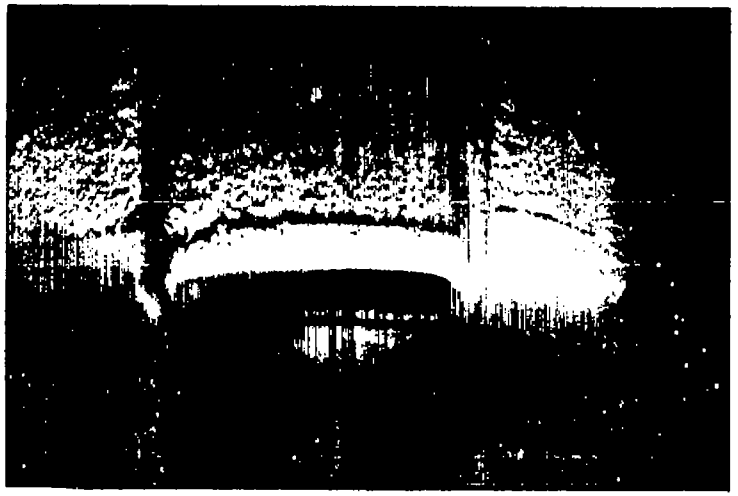

8 minutes

10 minutes

NACA
C-11958
8-17-45

Figure 17. - Progressive formation of rime ice on standard scoop. t, 15° F; W_c, 12,000 pounds per hour; W_e, 42 pounds per second; α, 0°; V, 200 miles per hour.

Front view

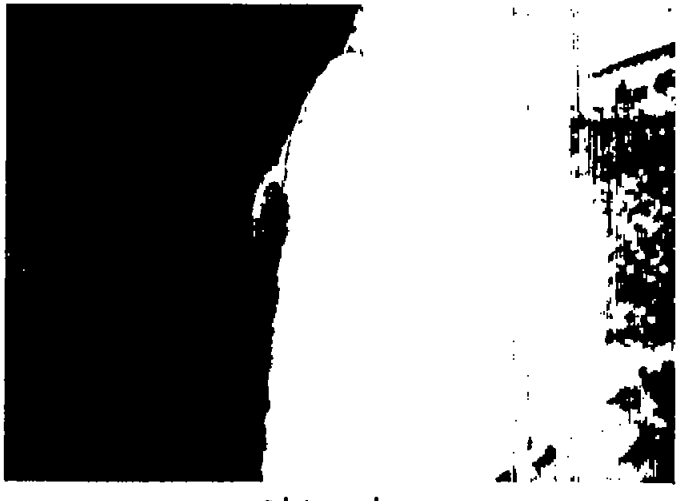

Side view

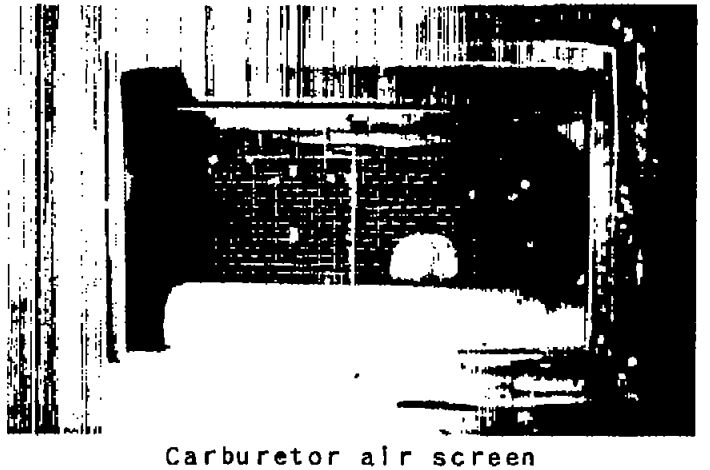

Carburetor air screen

(a) α, 8°; V, 160 miles per hour; 25-minute run.

Figure 18. - Heavy clear-ice formations on under-cowling scoop. t, 25° F, W_c, 12,000 pounds per hour; W_e, 42 pounds per second.

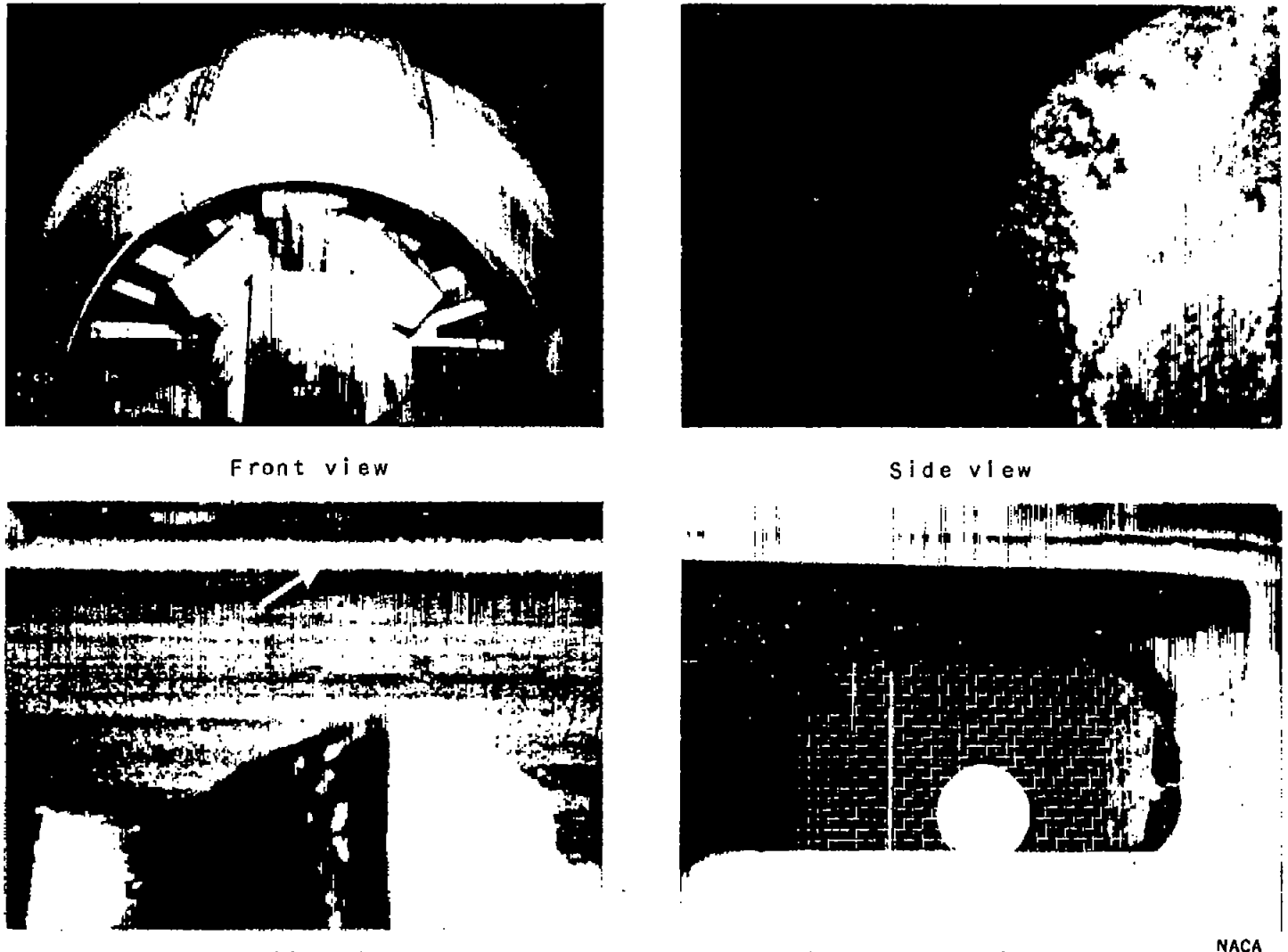

Front view

Side view

Inner lip of scoop

Carburetor air screen

NACA
C-10056
5-16-45

(b) α, 0°; V, 190 miles per hour; 20-minute run.

Figure 18. - Concluded. Heavy clear-ice formation on under-cowling scoop. t, 25° F; W_c, 12,000 pounds per hour; W_e, 42 pounds per second.

Front view

Side view

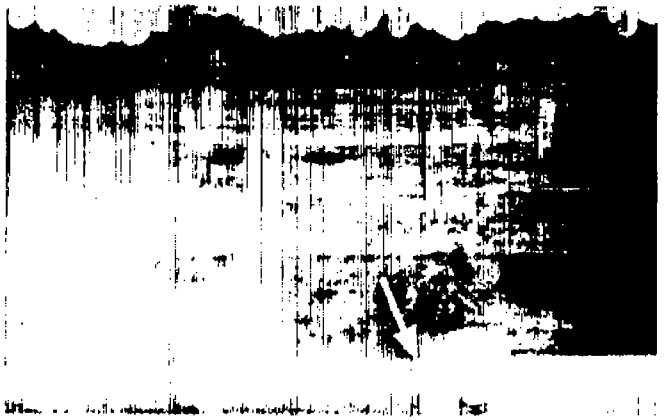

Inner and outer lips of scoop

Carburetor air screen

NACA
C-10058
5-16-45

(a) α, 8°; V, 160 miles per hour; 20-minute run.

Figure 19. - Rime-ice formations on under-cowling scoop. t, 15° F; W_c, 12,000 pounds per hour; W_e, 42 pounds per second.

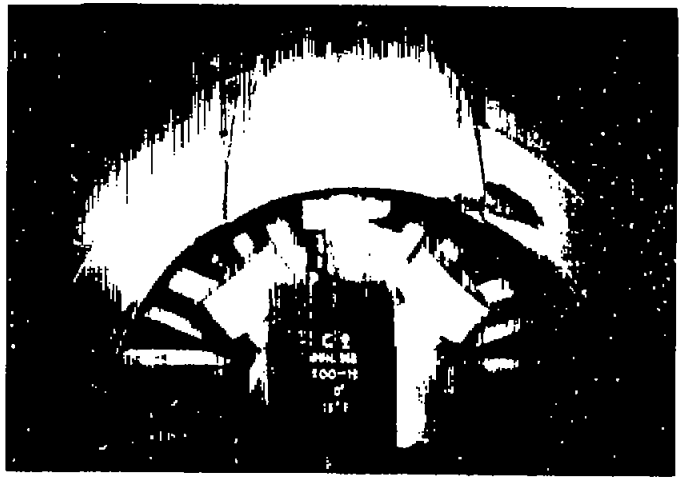

Front view

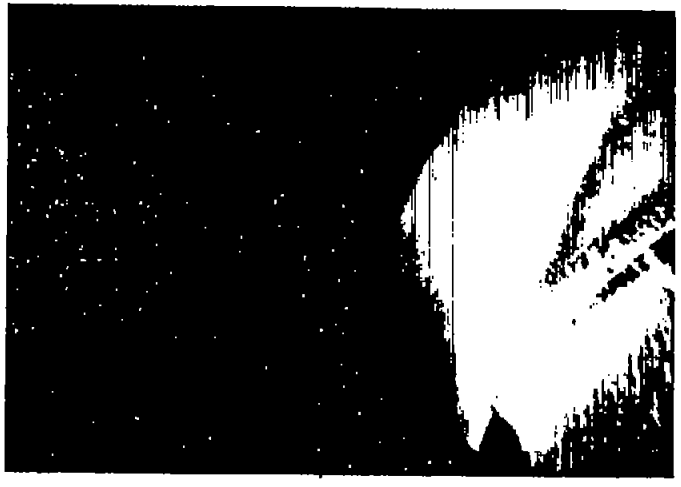

Side view

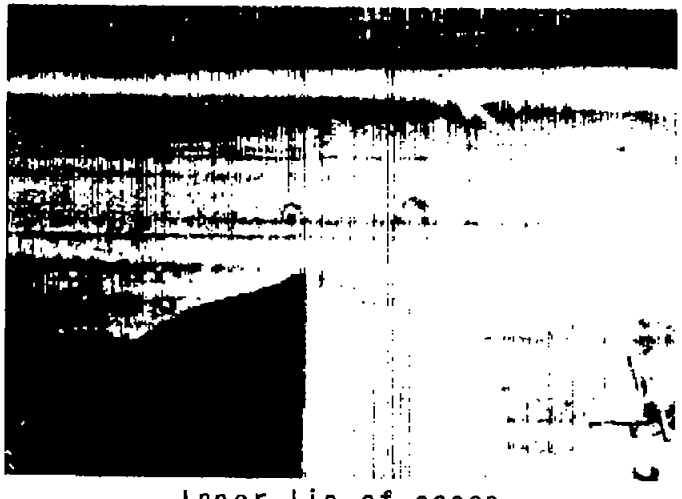

Inner lip of scoop

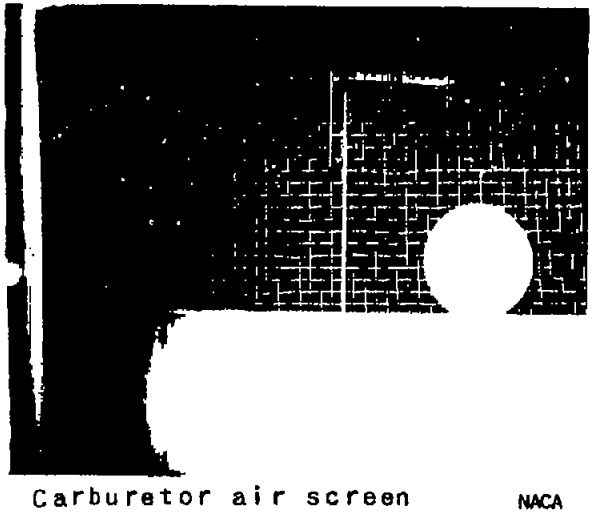

Carburetor air screen

NACA
C-10050
5-16-45

(b) α, 0°; V, 200 miles per hour; 15-minute run.

Figure 19. - Concluded. Rime-ice formations on the under-cowling scoop. t, 15° F; W_c, 12,000 pounds per hour; W_e, 42 pounds per second.

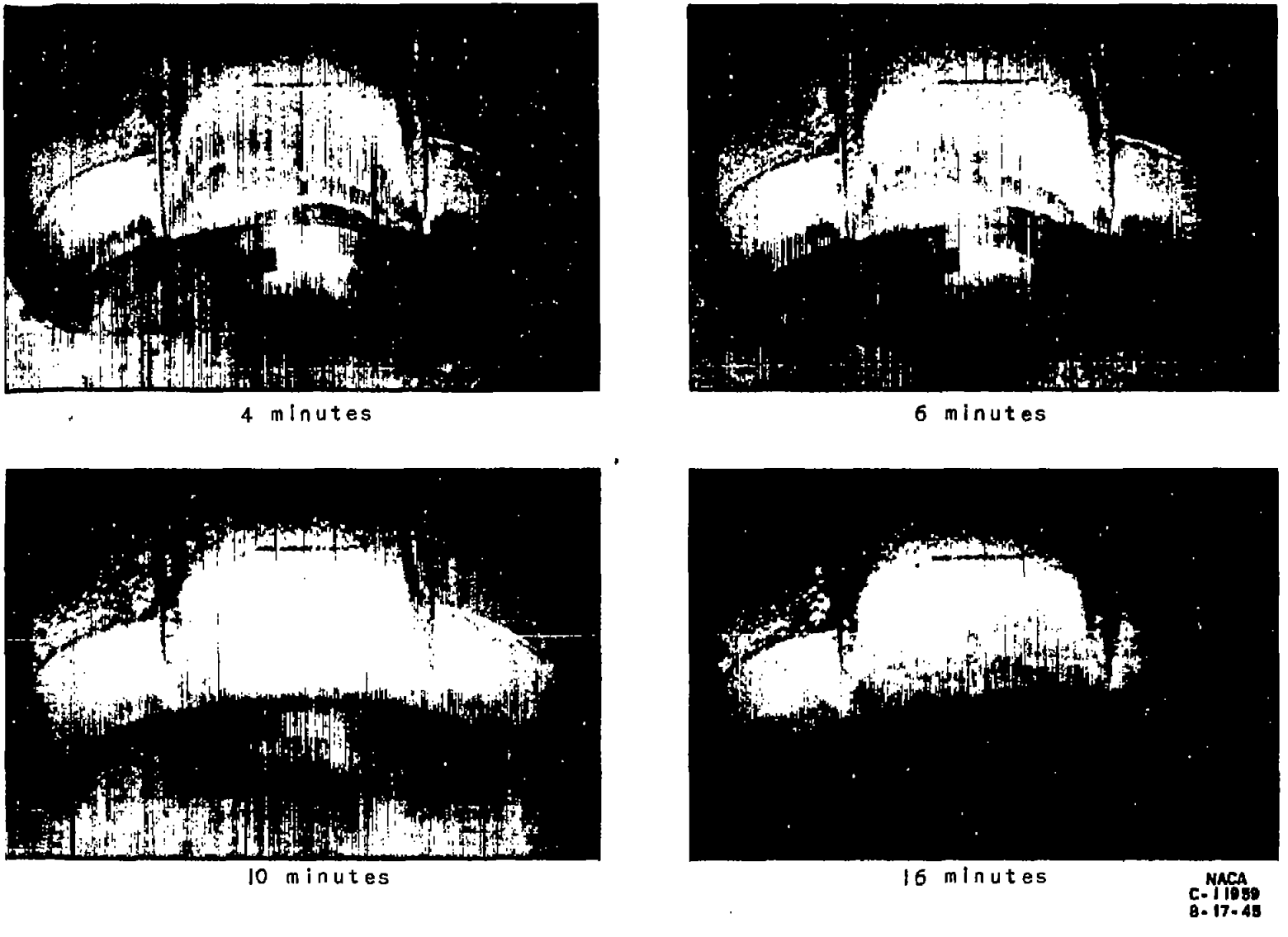

Figure 20. – Progressive formation of rime ice on under-cowling scoop. t, 15° F; W_c, 12,000 pounds per hour; W_e, 42 pounds per second; α, 8°; V, 160 miles per hour.

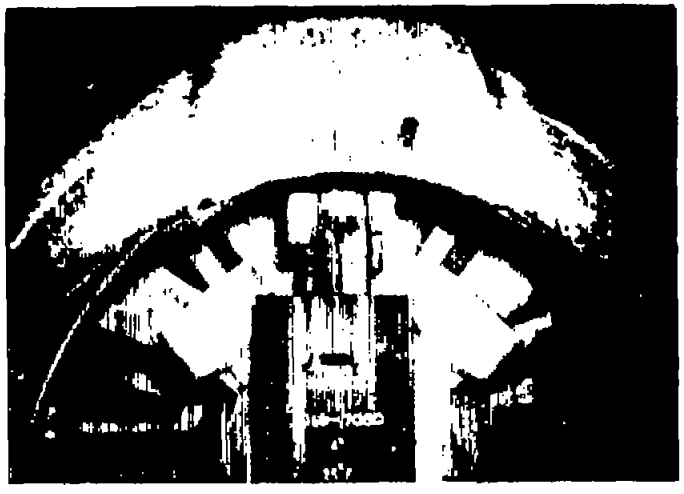

Front view

Side view

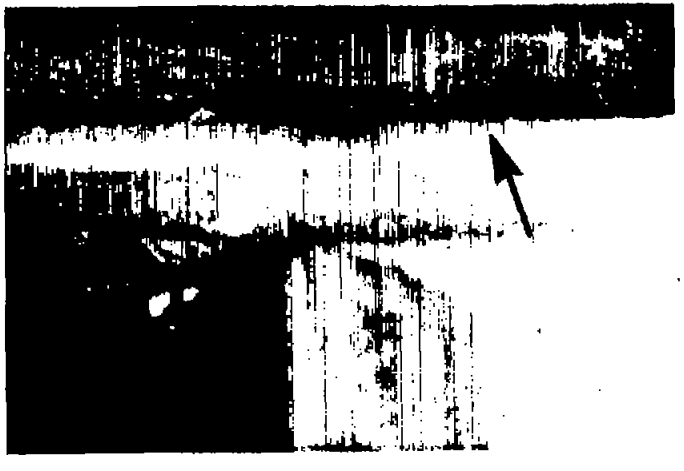

Inner lip of scoop

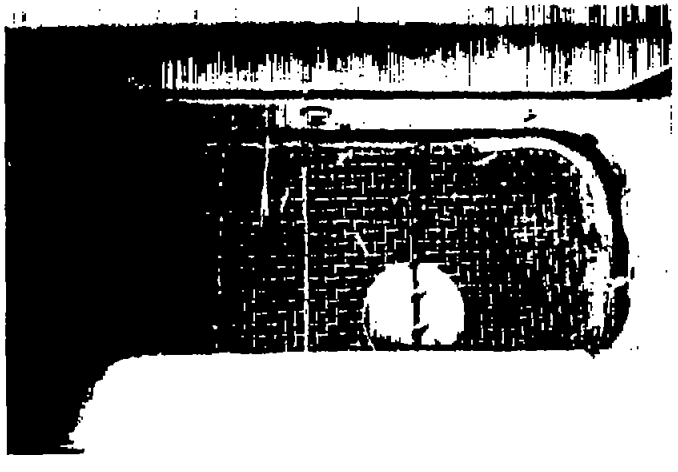

Carburetor air screen

NACA
C-10061
5-16-45

(a) t, 25° F; W_c, 7000 pounds per hour; W_a, 26 pounds per second; 10-minute run.

Figure 21. - Ice formations on modified under-cowling scoop. V, 160 miles per hour; α, 4°.

Three-quarter view

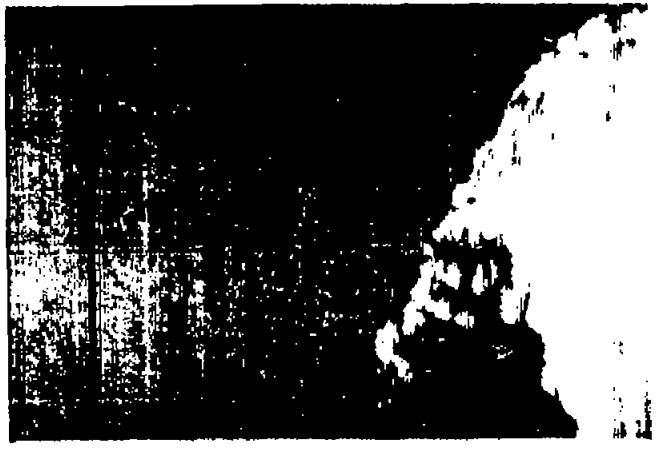

Side view

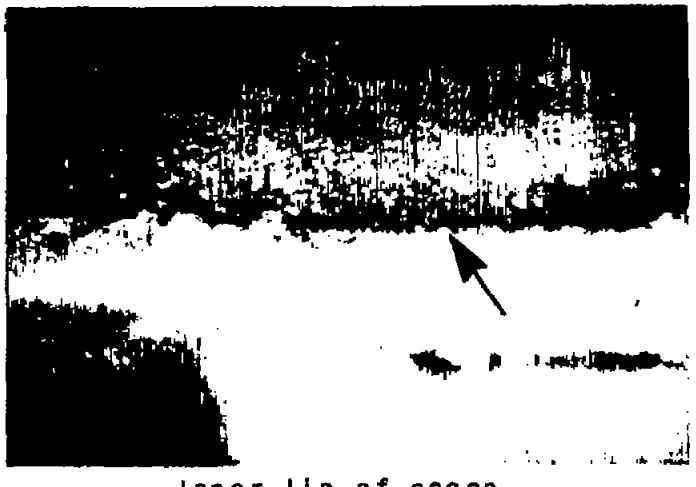

Inner lip of scoop

(b) t, 25° F; W_c, 12,000 pounds per hour; W_e, 42 pounds per second; 15-minute run.

Figure 21. - Continued. Ice formations on modified under-cowling scoop. V, 160 miles per hour; α, 4°.

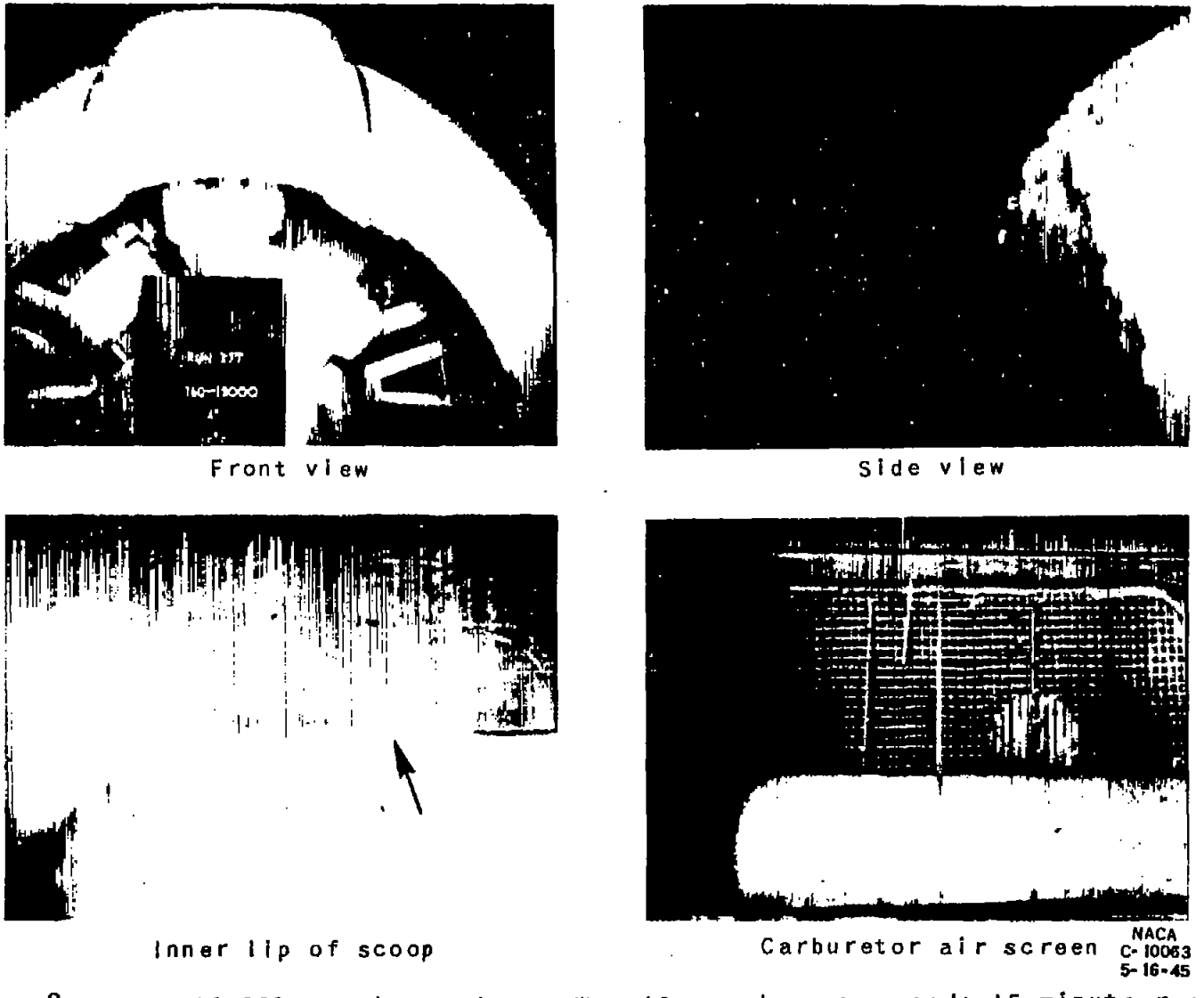

Front view

Side view

Inner lip of scoop

Carburetor air screen

NACA C-10063 5-16-45

(c) t, 15° F; W_c, 12,000 pounds per hour; W_a, 42 pounds per second; 15-minute run.

Figure 21. - Concluded. Ice formations on modified under-cowling scoop. V, 160 miles per hour; α, 4°.

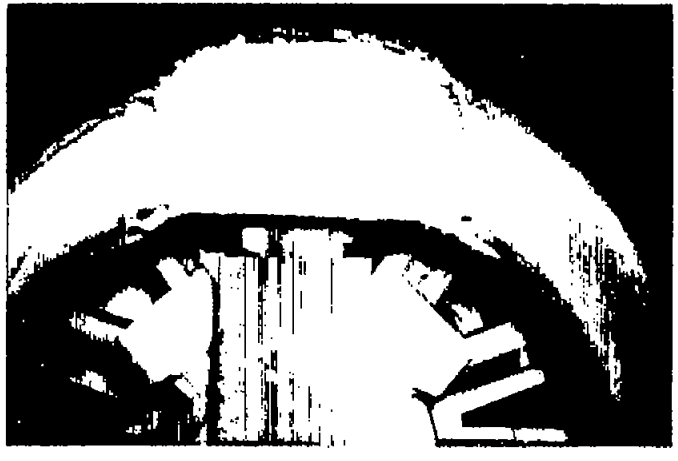

Front view

Side view

Three-quarter view

Carburetor air screen

NACA
C-10065
5-16-45

Figure 22. - Ice formations on combined standard and under-cowling scoop after 15-minute run. 16-mesh inlet screen; t, 25° F; W_c, 12,000 pounds per hour; W_e, 42 pounds per second; α, 4°; V, 160 miles per hour.

Fig. 22

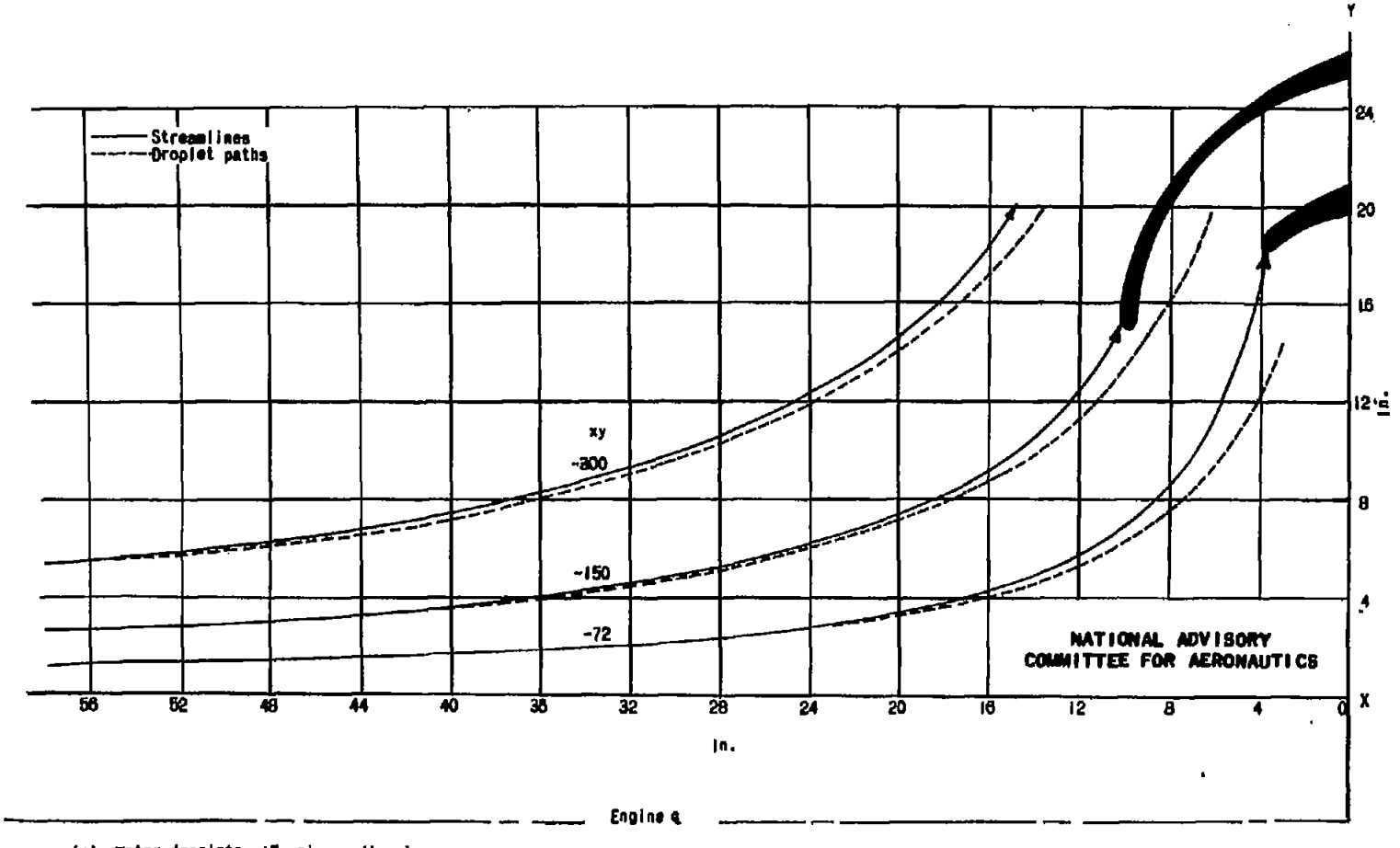

(a) Water droplets, 15-micron diameter.

Figure 23. - Theoretical paths of water droplets and streamline flow of the type $\psi = -xy$ with the outline of the under-cowling scoop arbitrarily superimposed. V_o, 300 feet per second.

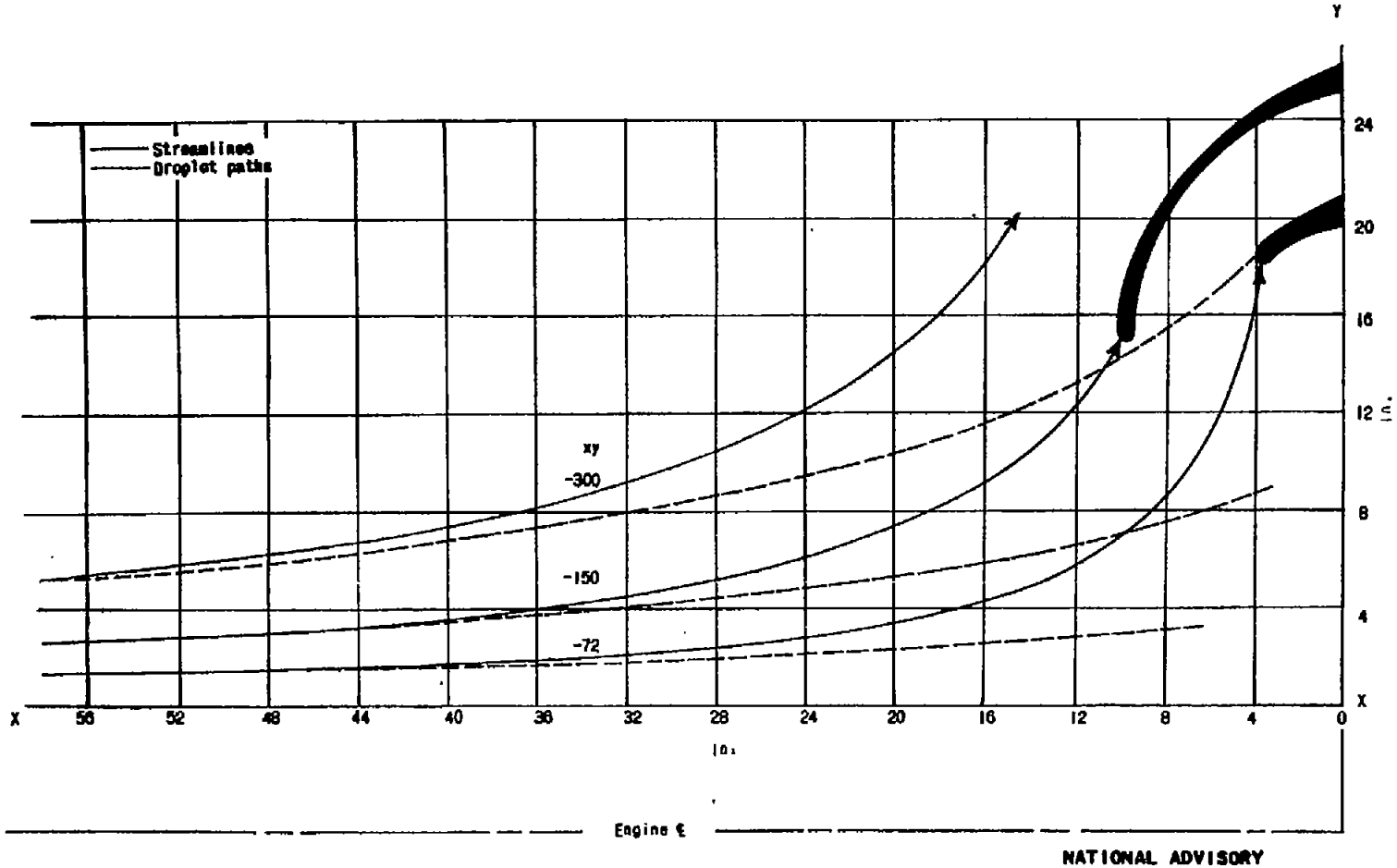

(b) Water droplets, 40-micron diameter.

NATIONAL ADVISORY
COMMITTEE FOR AERONAUTICS

Figure 23. - Concluded. Theoretical paths of water droplets and streamline flow of the type $\psi = -xy$ with the outline of the under-cowling scoop arbitrarily superimposed. V_0, 300 feet per second.